Journal of Marine Systems 239 (2023) 103853

Contents lists available at ScienceDirect

Journal of Marine Systems

journal homepage: www.elsevier.com/locate/jmarsys

Variability of pCO_2 and FCO_2 in the Mexican Pacific during 25 years

Coronado-Álvarez Luz de Lourdes Aurora [a], Hernández-Ayón José Martín [a,*], Delgado-Contreras Juan Antonio [b], Durazo Reginaldo [c], Espinosa-Carreón T. Leticia [d], Norzagaray-López Orión [a], Sosa-Ávalos Ramón [e], Chapa-Balcorta Cecilia [f]

[a] Instituto de Investigaciones Oceanológicas, Universidad Autónoma de Baja California, Ensenada, Baja California, Mexico
[b] Tecnológico Nacional de México/Instituto Tecnológico de Guaymas, Avenida Tecnológico km 4, Sector Las Playitas, C.P. 85480 Guaymas, Sonora, Mexico
[c] Facultad de Ciencias Marinas, Universidad Autónoma de Baja California, Ensenada, Baja California, Mexico
[d] Instituto Politécnico Nacional, CIIDIR- SINALOA, Guasave, Sinaloa, Mexico
[e] Universidad de Colima, Centro Universitario de Investigaciones Oceanológicas, Carretera Manzanillo-Barra de Navidad, Colima, Mexico
[f] Facultad de Ciencias Marinas, Universidad del Mar, Oaxaca, Mexico

A R T I C L E I N F O

Keywords:
Cabo Corrientes
California current system
El Niño/La Niña
FCO_2
Gulf of Tehuantepec
pCO_2
Variability
Mexican Pacific

A B S T R A C T

Oceanographic features acting on different spatial-temporal scales influence the variation in the partial pressure of CO_2 (pCO_2) and ocean-atmosphere CO_2 flux (FCO_2). In this work, we regionally characterize regions of variability in the Mexican Pacific (MP) based on these chemical properties. We also evaluate the seasonal and interannual changes of each region: in the California Current System (CCS), Cabo Corrientes (CC), and Gulf of Tehuantepec (GT) regions. Sea surface temperature (SST), salinity, wind, pCO_2, and FCO_2 data from 1993 to 2018 were analyzed. Bayesian *t*-tests (95% credibility intervals) determined showed that the three regions had high probabilities of being different. Typical FCO_2 values in the CCS were higher (−27.6–29.8 mmol C m^{-2} d^{-1}) than those of the CC and GT regions (−19.9–25.8 and − 11.8–12.5 mmol C m^{-2} d^{-1}, respectively). The highest positive seasonal variation of FCO_2 (mean ± standard deviation) was found in the CCS and CC (~4.6 ± 4.2 mmol C m^{-2} d^{-1}) regions during spring, and in the GT region (1.2 ± 2 mmol C m^{-2} d^{-1}) in autumn due to the strong northerly winds. It was found that during ENSO conditions the MP was a source (4.0 and 3.9 mol C m^{-2} y^{-1} for El Niño and La Niña, respectively), although on average over the last 25 years included in the study the MP acted as a slight-CO_2 sink (~10.9 ± 0.005 mol C m^{-2}).

1. Introduction

Anthropogenic activities (vg., deforestation, land use change, cement production), as well as the biogeochemical processes that participate (or interact) with the carbon cycle, influence the variability of atmospheric CO_2 concentrations (Falkowski et al., 2000). When atmospheric CO_2 encounters the ocean, it forms part of the carbonate system, which can be affected by various physical, chemical, and biological drivers (i.e., affecting the amount of inorganic carbon species; DeGrandpe et al., 1998). Thus, understanding the dynamics of this greenhouse gas in the ocean is extremely important given its role as a long-term climate regulator (Reid et al., 2009), particularly in a global warming scenario. As a whole, the ocean acts as a CO_2 sink (Sabine et al., 2004) and absorbs around 26% of anthropogenic emissions (Friedlingstein et al., 2021), although both magnitude and trend vary according to the season of the year and geographic region. Overall, the Eastern Tropical Pacific is considered an emitting source of CO_{2gas} to the atmosphere (Chavez et al., 2007; Takahashi et al., 2009), with high interannual variability (Feely et al., 2002; Park et al., 2010).

At the sea surface, the partial pressure of CO_2 (pCO_2) is affected by several processes, such as photosynthesis, respiration, upwelling, changes in temperature, water-column mixing, and mesoscale or sub-mesoscale structures, some of them covarying simultaneously (DeGrandpe et al., 1998; Chavez et al., 2007; Chiodi et al., 2019). Although substantial efforts have been made to understand the global variability (mostly at seasonal and interannual scales) in pCO_2 and CO_2 fluxes at the ocean-atmosphere interface (FCO_2), only around 50% of the uncertainty in net annual ocean FCO_2 estimates based on in-situ measurements (Sutton et al., 2017) has been reduced in different spatial-temporal scales. This allows reducing the variability of gridded

* Corresponding author.
E-mail address: jmartin@uabc.edu.mx (H.-A.J. Martín).

https://doi.org/10.1016/j.jmarsys.2022.103853
Received 10 March 2022; Received in revised form 5 December 2022; Accepted 15 December 2022
Available online 17 December 2022
0924-7963/

products (Bakker et al., 2014) because cells without pCO2 observations are left empty (Bakker et al., 2016). Part of this uncertainty at regional and local scales is the result of multiple processes that modulate the ocean-atmosphere gas exchange at different time scales, ranging from hours to decades (Chavez et al., 2007; Coronado-Álvarez et al., 2017; Sutton et al., 2017). Thus, there is a need to better understand the factors that drive the variability in pCO_2 and FCO_2 in coastal and oceanic regions at different spatio-temporal scales (Sutton et al., 2017).

South of 35° N, the Pacific has been reported to be a slight source of CO_2 (Chavez et al., 2007; Takahashi et al., 2009). The seasonal, interannual and decadal variability of pCO_2 and FCO_2 in this area over the last decade have generated great research interest (Hales et al., 2012; Nakaoka et al., 2013; Chiodi et al., 2019; Yasunaka et al., 2014, 2019). However, questions remain regarding the dynamics of FCO_2 at various spatio-temporal scales. A unique area in the Pacific Ocean, characterized by the commingling water masses of subarctic, tropical and equatorial origins, is the region of the Mexican Pacific (MP; ~9–34° N, ~86–125° W; Fig. 1). Particular oceanographic conditions in summer arise from the confluence of the equatorward flowing California Current water of subarctic origin, with the poleward flows of Transitional Water (TW) and Tropical Surface Water (TSW) up to ~27° N towards the Baja California peninsula (Trucco-Pignata et al., 2019; Portela et al., 2016).

The tropical Mexican Pacific (south of ~22.5°N) is located in one of the largest oxygen minimum zones (OMZ) in the world (dissolved oxygen values of <20 μmol kg^{-1} are located as shallow as ~40 m depth, although these low values are found typically in deepest waters at 400 m depth). This OMZ is considered a warm water pool (Cepeda-Morales et al., 2013) that has intensified and expanded due to increases in atmospheric CO_2 (Trucco-Pignata et al., 2019). In this work, the description of both pCO_2 and FCO_2 of the MP has been subdivided in three subregions: the California Current System (CCS), Cabo Corrientes (CC),

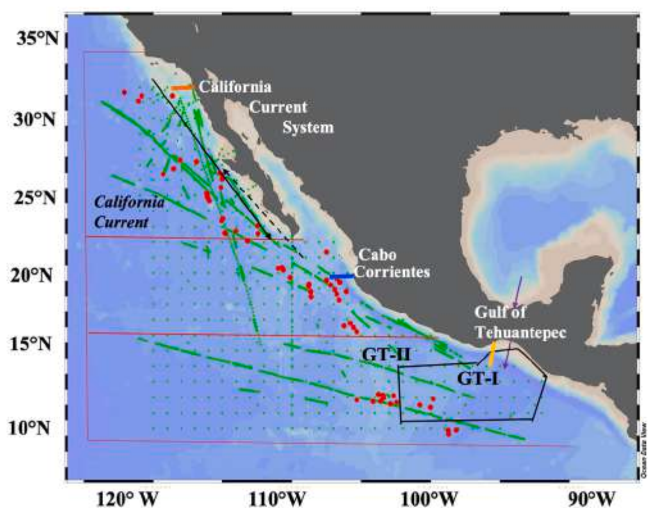

Fig. 1. Data points (green dots) in the three regions of the Mexican Pacific (red polygons): the California Current System (CCS), Cabo Corrientes (CC), and Gulf of Tehuantepec (GT) regions. Sea surface temperature (SST), salinity, and partial pressure of CO_2 (pCO_2) data cover the period from 1993 to 2018 and were obtained from various databases (measurements and gridded products). The California Current mean spring (summer) circulation is represented by a black (dashed) arrow. The purple arrows represent the direction of Tehuano winds (November to March) in the GT. The polygon delimited by black lines indicates the area of the GT under the influence of Tehuano winds (GT-I). The remaining area of the GT with the tropical condition is referred to as GT-II. The red dots are the hydrographic stations for the estimation of the stratification parameter (Φ; J m^{-3}). The orange, blue and yellow coastal solid lines represent the transects of each region at 33° (CCS), 20° (CC), and 15° N (GT-I), respectively. (For interpretation of the references to colour in this figure legend, the reader is referred to the web version of this article.)

and the Gulf of Tehuantepec (GT) (Durazo and Baumgartner, 2002; Flores-Morales et al., 2009; Fiedler et al., 2013; Fiedler and Lavín, 2016).

The CCS region is characterized by the equatorward flow of subarctic water through the California Current. This region is also characterized by the presence of wind-driven upwelling in spring. In winter, the southern limit of the California Current can be found at ~20° N, while this retracts to ~27° N in summer (Lynn and Simpson, 1987; Durazo, 2015; Fig. 1). Additionally, the presence of a latitudinal gradient and seasonal variations in sea temperature, pCO_2, and FCO_2 have been documented in this region (Hernández-Ayón et al., 2010; De la Cruz-Orozco et al., 2010; Mariano-Matías et al., 2016). Measurements of pCO_2 in the southern portion of the California Current using a moored autonomous high frequency sensor Moored Autonomous pCO_2, ($MAPCO_2$; 31.6° N, 116.6° W; https://www.pmel.noaa.gov/co2/file/MAPCO2) have found that pCO_2 varies according to the time of year (Muñoz-Anderson et al., 2015), indicating that the CCS appears to act as both a source and sink of CO_2, although in different magnitudes. However, at an annual scale, i.e., integrating those measurements over 2009, indicated that the CCS was a source of CO_2 to the atmosphere (0.3 ± 0.06 mol C m^{-2} y^{-1}). In addition, Coronado-Álvarez et al. (2017) analyzed the $MAPCO_2$ time series from 2008 to 2015 and identified several drivers that influenced the variation in FCO_2, such as upwelling, El Niño and La Niña events, and high-frequency variability, describing how this region went from being a CO_2 source to a CO_2 sink in a matter of hours.

In the CC region (~20° N; Fig. 1) within the tropical Mexican Pacific, warm ocean temperatures (>20 °C) result in notable water-column stratification. For this region, the nominal value of the stratification parameter (Φ, 0–300 m) is ~1200 J m^{-3}, indicating a well-stratified water column (Franco et al., 2014; Trucco-Pignata et al., 2019). Seasonal upwellings occur here, although a higher amount of energy is required for subsurface water to reach the surface compared with that of the CCS. In addition, latitudinal and seasonal variations in FCO_2 have been reported in the CC region by Franco et al. (2014), signalling November as a source (2.5 mmol C m^{-2} d^{-1}) and August as varying between −4.4 and 3.3 mmol C m^{-2} d^{-1}.

To the southeast of the CC lies the GT region, which is seasonally influenced by strong northerly winds (named Tehuanos) in autumn and winter (November to March) driven by sea level atmospheric pressure gradients between the Gulf of Mexico and the Mexican Pacific across the Isthmus of Tehuantepec promoting strong mixing and upwelling conditions (Fiedler and Lavín, 2016). During the remainder of the year, warm water temperatures (~25 °C) prevail in the region. Seasonally, spatial variations in FCO_2 (0–40 mmol C m^{-2} d^{-1}) (Chapa-Balcorta et al., 2015) and notable stratification (1200 J m^{-3}; Fiedler et al., 2013) have also been reported.

Given the different oceanographic conditions and subregions within the MP, FCO_2 dynamics vary greatly over diurnal to seasonal scales (Coronado-Álvarez et al., 2017), making it difficult to estimate and understand FCO_2 controls (Friederich et al., 2008). Moreover, other phenomena that influence greater spatial and temporal scales also influence FCO_2 dynamics, such as the El Niño Southern Oscillation (ENSO). These factors must be addressed to understand FCO_2 variability in the MP.

Despite the worldwide efforts to characterize the oceanic regions as either sources or sinks of CO_2 (Takahashi et al., 2009) and understand the physical, chemical, and biological factors that influence pCO_2 and FCO_2 variability (Pennington et al., 2010; Coronado-Álvarez et al., 2017; Sutton et al., 2017), many information gaps remain, likely due to a lack of data and their interpretation. In the MP, Chapa-Balcorta et al. (2019) indicated that a greater number of studies have focused on the CCS, while scarce data is available for the CC and GT regions. The main reason for the latter lies in the challenges associated with sampling in these regions, especially difficult during fall-winter due to the presence of strong northerly Tehuano winds. Studies conducted in the tropical

Mexican Pacific date from ~2009 to the present; however, the oceanographic cruises covered small areas, and thus a small amount of data has been collected. Therefore, being able to identify each driver that influences the variability of FCO_2 at various spatio-temporal scales with limited data is a complex task.

In this study, we used international databases from different sources, vg., National Oceanic and Atmospheric Administration (NOAA, 2018), and Lamont-Doherty Earth Observatory (Takahashi et al., 2009), which were available for the CCS, CC, and GT regions of the MP. The information was used to (1) Characterize the different regions in terms of analysis of chemical variables, (2) Quantify the seasonal and interannual variation in pCO_2 and FCO_2, and (3) Estimate the net carbon flux in the MP over the last 25 years (1993–2018) in order to assess whether the MP is a net source of CO_2 to the atmosphere.

2. Materials and methods

Data on sea surface temperature (SST; °C), salinity, and pCO_2 (μatm) from oceanographic campaigns conducted in the CCS, CC, and GT regions of the MP from the period 1993 to 2018 (Fig. 1), were obtained from the following sources: (1) the Ocean Acidification Data Stewardship project from NOAA (NOAA, 2018; https://www.ncei.noaa.gov/access/oads/), (2) the Global Ocean Data Analysis Project (GLODAP_2020; https://www.glodap.info/; Lauvset et al., 2021); (3) the Lamont-Doherty Earth Observatory (LDEO; https://www.ldeo.columbia.edu/research/databases-repositories; Takahashi et al., 2017); (4) the Surface Ocean CO₂ Atlas (SOCAT; https://www.socat.info/; Bakker et al., 2016). Also, we used gridded data because the measurements in some zones of the study area are scarce. And we wanted to have thousands of data with the aim that our results would be robust; this kind of information is described as follows: (5) gridded FCO_2 data was used from Valsala and Maksyutov (2010) (Supplementary Material, SM; SM00_Database_MP); these authors referred that the error of their estimation was similar to reported by Takahashi et al. (2009); and (6) pCO_2 gridded monthly data from Takahashi et al. (2014). Oceanographic cruise codes were considered to ensure no duplicated information, this was measurements; however, it is important that the gridded data is an estimation of measurements around the study area. A total of 15,000 data points, which merge gridded and measurements. However, as quality control of data from repositories, we used the data-quality flags defined by the World Ocean Database (https://www.nodc.noaa.gov/OC5/WOD/CODES/Definition_of_Quality_Flags.html). Data with "bad" or "questionable" quality code flags were excluded. After this filtering, ~ 13,500 data were included in the integrated database. It is important to mention that the data point was occupied more than once; therefore, the number of data differs among seasons, with 18,816, 20,711, 12,209, and 15,677 for winter, spring, summer, and autumn, respectively (SM1). Although our time series were assembled from different databases, it was assumed that original data had been subjected to rigorous quality control to verify precision and accuracy (overall average accuracy values $< \pm 5$ μatm), according to assessments of pCO_2 accuracy from SOCAT (Bakker et al., 2016); however, the gridded data had different accuracy and variability in comparison with measurements, that was mentioned and discussed in the results and discussion sections.

This study aimed to identify the drivers of the changes in pCO_2 and FCO_2; therefore, the variations in satellite-derived SST_{sat} (°C; NASA, 2021a) and chlorophyll-a (Chl_{sat}; mg m^{-3}; NASA, 2021b) were analyzed seasonally to identify whether they corresponded to the fluctuations in the first two variables. Additionally, in-situ chlorophyll-a (Chl_{insitu}) data from various oceanographic surveys compiled by Soppa et al. (2017) were used to associate changes in the chlorophyll-a concentration with variations in FCO_2. Satellite data (SST_{sat} and Chl_{sat}) were obtained from the Modis-Aqua sensor and included weekly compositions spanning 2002 to 2018 (level L3 and 4 × 4 km resolution). In addition, daily-satellite images of absolute dynamic topography (ADT; cm) were obtained from the Copernicus Marine Environment Monitoring Service (CMEMS, 2020; https://cds.climate.copernicus.eu/). This daily data spanned from 1993 to 2018 and had a spatial resolution of 0.25°.

Considering that ENSO conditions imprint its variability at an interannual scale in the Pacific (Trucco-Pignata et al., 2019), the Oceanic El Niño Index (ONI) was used to identify the strongest El Niño/La Niña events recorded during the study period (https://origin.cpc.ncep.noaa.gov/products/analysis_monitoring/ensostuff/ONI_v5.php). Various ENSO events were recorded during the study period 1993–2018, although temperature, salinity, pCO_2, and FCO_2 data were only available for three El Niño events in 1994 (moderate), 1997–1998, and 2015–2016, and one La Niña event in 1998–2000. The data points (concluding gridded and measurements) per event were different, with ~550 and ~ 500 stations for warm and cold anomalies, respectively; data points were distributed from south to north, although with much less coverage from east to west (for more detailed data point locations see SM11 and SM12). Regional fluxes were integrated into each recorded event. In order to remove seasonality, monthly long-term climatological averages (excluding ENSO years) of SST, pCO_2, and FCO_2 were subtracted from the original data values. A similar procedure was applied to satellite data to obtain anomalies of SST_{sat}, ADT, and Chl_{sat}.

The stratification parameter (Φ; J m^{-3}), which is a measure of the stratification as it reflects the amount of energy required to completely mix the water column, was estimated between the surface and 300 m depth according to Simpson (1981). Density profiles derived from temperature and salinity recorded at 62 oceanographic stations distributed throughout the MP were used to calculate Φ. Casts selected were from March–May (2005) (CCS), November–June (2005–2006) (CC), and October–November (2006) (GT) (Fig. 1; 10 to 33° N and 96 to 120° W; (https://www.ncei.noaa.gov/access/world-ocean-database/datawodgeo.html; Boyer et al., 2018).

In addition, FCO_2 (mmol C m^{-2} d^{-1}) values were calculated from in-situ SST, salinity, wind, and pCO_2 (gridded and measurements) data using Eq. (1) proposed by Liss and Merlivat (1986):

$FCO_2 = k\alpha\Delta pCO_2$ (1)

where k is the gas transfer velocity which is a function of the wind speed (U), for which the transfer coefficient proposed by Wanninkhof (2014) was used. The transfer velocity is expressed as $k = 0.251(Sc/660)^{0.5} \times U^2$, and Sc is the Schmidt number as a function of temperature (for more details see Wanninkhof, 2014), α is the solubility of CO_2 in the ocean, a function of temperature and salinity (Weiss, 1974), and ΔpCO_2 is the difference between pCO_2 at the ocean's surface and the atmosphere (ΔpCO_2; $\Delta pCO_2 = pCO_2 - pCO_{2A}$). To calculate FCO_2, monthly atmospheric pCO_2 values were obtained from the Mauna Loa Observatory in Hawaii (19.53° N and 155.57° W; Dr. Pieter Tans, NOAA/GML; https://gml.noaa.gov/ccgg/trends/gl_data.html) and the Scripps Institution of Oceanography (Dr. Ralph Keeling; https://scrippsco2.ucsd.edu/data/atmospheric_co2/primary_mlo_co2_record.html). These monthly air pCO_2 values were obtained for the same dates as our in-situ pCO_2 measurements. Also, to calculate FCO_2 (Eq. 1) for each oceanographic station included, we used the closest daily average wind data (m s^{-1}) provided by the NOAA repository (https://psl.noaa.gov/data/gridded/data.ncep.reanalysis.html; Kalnay et al., 1996). Gridded FCO_2 data that we used were estimated with the coefficient of Wanninkhof (1992); this fact implies a little difference with FCO_2 estimated with pCO_2 values (gridded and measurements) used in this study with Wanninkhof (2014) coefficient. The difference is around 20% (Wanninkhof, 2014), this was mentioned in the discussion section.

Despite the effort to bring collected thousands of measured and gridded pCO_2 and FCO_2 data, our time series (1993 to 2018) has gaps, which are mentioned in the following sections and considered in the interpretation of our findings. This indicates the need for measurements in the study area with greater spatial and temporal coverage to have an optimal approach process that occurs in it.

In order to quantify the effect of temperature on pCO_2 (only measurements without gridded data), a pCO_2 anomaly was calculated as the

pCO_2 value minus the calculated temperature effect on pCO_2 ($pCO_{2\,(norm)}$). This term was calculated with the annual mean pCO_2 (i.e., 392, 376, and 382 µatm values for CCS, CC, and GT region, respectively), and the difference between the temperature measurements (T_{obs}) and the annual mean (T_{mean}) temperature by region (18.6, 25.1 and 28.1 °C for CCS, CC, and GT, correspondingly), namely:

$$pCO_{2(norm)} = annual\ mean\ pCO_2 \times\ exp\ [0.0423(T_{obs} - T_{annual\ mean})] \quad (2)$$

Due to the large dispersion of data values over a large geographic area, the statistical assumption of normality was not met. For this reason, we opted for Bayesian inference, as the normality assumption is not required because Bayesian inference is based on probabilities. Bayesian *t*-tests were used to evaluate the probability of differences between two sets of data: (1) contrasting among regions of the study area and (2) contrasting among the four seasons. For this analysis, 95% credibility intervals criteria were considered. Analyses were conducted using R-Studio and the 'BEST: Bayesian Estimation Supersedes the t-Test' package. A Bayesian estimator minimizes the loss of a punctual function (Kelter, 2020). For this reason, we performed our tests using the medians given the large dispersion of data values (Held and Sabanés, 2014), and also because this type of analysis strengthened the regionalization of the MP (Kruschke, 2013). These statistical analyses were performed to test for differences in SST, pCO_2, FCO_2, ADT, and Chl_{sat} data among regions and seasons (January – March, April – June, July – September, and October–December, for winter, spring, summer, and autumn, respectively).

In contrast to other studies that have estimated the variability of FCO_2 in the MP region and worldwide, our results are presented as seasonal average values of each region with the corresponding, rather large, standard deviations. Our results were presented as follows: fluxes results (gridded and calculated) were integrated and re-scaled (mol m^{-2} y^{-1}, or g m^{-2} y^{-1}) for the different spatial (study region) and temporal (seasonal and annual) scales studied. Integration of FCO_2 values was performed in several ways. FCO_2 seasonal means were estimated using the monthly means of whole database per region. Yearly means were obtained by estimating the FCO_2 for the whole MP and then dividing by the total number of years (25) of the data set.

3. Results

3.1. Physical Onset

In-situ SST long-term (1993–2018) data means by region and season were within the ranges previously reported (Table 1; Durazo et al., 2001, Fiedler et al., 2013). Temperature ranges for the CCS, CC, and GT regions were 12.4–29.3, 18.1–30.6, and 19.7–31.5 °C, respectively (Fig. 2a). Typical spring to summer warming of the surface water was observed, with corresponding temperature decreases in autumn and winter. In addition, the temperature of the wind-influenced area of the GT (~10–15° N; Chapa-Balcorta et al., 2015; Fiedler et al., 2013) further decreases in autumn and winter, with a marked spatial pattern of temperatures increasing from onshore (~24 °C) to offshore (~28 °C; Supplementary Material 2, SM2).

The ADT seasonal climatologies derived from the 25 years of satellite images (SM3) showed that, at this time scale, sea level changed in the three regions of the MP. Also, lower values (~40 cm) were observed in the north and higher values in the south (~60–100 cm in the CC and GT). Particularly, the offshore transport of coastal waters in the GT caused by Tehuano winds was observed in autumn and winter (area within 10–15° N and 92–100° W), and led to values of ~50 cm, which were a consequence of the highest wind magnitudes for this season and region. In the case of the CCS, the highest sea level values (~60 cm) were observed in winter (related to winds up to ~8 m s^{-1}). Similarly, these highest wind values were observed in the GT during autumn and winter (wind >15 m s^{-1}) when Tehuano wind conditions result in lower SST (SM2) and ADT values (SM3).

Table 1
Mean (± standard deviation) of sea surface temperature (SST), partial pressure of CO_2 in the ocean' surface (pCO_2), the difference of pCO_2 between the ocean and atmosphere (ΔpCO_2), and the flux of CO_2 at the ocean-atmosphere boundary (FCO_2) by regions and seasons. Regions included are the California Current System (CCS), Cabo Corrientes (CC), and Gulf of Tehuantepec, the latter with Tehuano wind influence (GT-I) and tropical conditions (GT-II). Season includes spring (Sp), summer (Sm), autumn (Au), and winter (Win).

Region	Season	SST (°C)	pCO_2 (µatm)	ΔpCO_2 (µatm)	Wind (m s^{-1})	FCO_2 (mmol C m^{-2} d^{-1})
CCS	*Sp*	17.7 ± 1.2	410 ± 28	30 ± 25	3.7 ± 2.0	4.6 ± 4.2
	Sm	23.9 ± 3.6	391 ± 22	−7 ± 19	3.8 ± 2.8	−1.6 ± 6.0
	Au	23.6 ± 3.7	401 ± 22	20 ± 16	3.8 ± 3.0	3.2 ± 3.2
	Win	18.6 ± 1.2	380 ± 12	−15 ± 16	4.0 ± 2.2	−4.3 ± 4.2
CC	*Sp*	23.4 ± 2.7	407 ± 22	36 ± 24	7.6 ± 4.4	4.2 ± 3.0
	Sm	29.2 ± 1.0	363 ± 40	−22 ± 40	2.7 ± 1.9	−4.0 ± 7.7
	Au	27.0 ± 1.8	381 ± 33	−4 ± 31	5.3 ± 4.2	0.1 ± 4.2
	Win	22.9 ± 1.8	359 ± 17	−32 ± 22	3.0 ± 2.0	−5.7 ± 3.0
GT-I	*Sp*	28.7 ± 1.2	388 ± 40	1 ± 32	10.0 ± 4.0	0.3 ± 3.6
	Sm	30.0 ± 0.4	372 ± 20	3 ± 19	7.5 ± 5.5	0.7 ± 2.0
	Au	27.7 ± 2.4	416.9 ± 12	34 ± 17	14.1 ± 2.5	4.3 ± 2.2
	Win	25.8 ± 0.2	434.8 ± 10	61.4 ± 10	11.0 ± 1.0	8.9 ± 1.5
GT-II	*Sp*	28.5 ± 1.5	387 ± 39	4 ± 29	9.1 ± 4.0	0.5 ± 3.4
	Sm	30.2 ± 0.5	386 ± 7	12 ± 5	2.5 ± 1.9	1.3 ± 0.6
	Au	28.4 ± 1.2	383 ± 16	4 ± 16	7.0 ± 3.2	0.5 ± 2.0
	Win	26.3 ± 1.5	379 ± 21	−16 ± 13	7.0 ± 3.0	−1.8 ± 1.8

3.2. pCO_2

Overall, we observed that pCO_2 varied seasonally, and the ranges of the variability of pCO_2 were between ~200 and 500 µatm in all regions. However, the highest and lowest values were present mainly in two different seasons, spring and autumn, correspondingly, as described next. In the CCS, maximum (495 µatm) and minimum (280 µatm) values were present in spring (average of 410 ± 28 µatm), with an annual mean of 391 ± 23 µatm. Similarly, in the CC, the highest (499 µatm) and lowest (280 µatm) values were present in spring (mean of 407 ± 22; Fig. 2b, Table 1; SM5), with an annual mean of 376 ± 32 µatm. The GT region was divided into two areas: a zone under the direct influence of Tehuano winds (GT-I; 10–15° N, 92–100° W) and another zone composed of all areas with tropical conditions (GT-II; 9–10° and 15 to 16.5° N). In GT-I, the pCO_2 values fluctuated between 286 and 500 µatm in spring and autumn, respectively, while minimum and maximum averages were obtained in summer (372 ± 20 µatm) and winter (434.8 ± 10 µatm) (Table 1; Fig. 2b, SM4). Correspondingly, the seasonal pCO_2 averages for summer and winter in GT-II were 386 ± 7 and 379 ± 21 µatm, respectively (Fig. 2b, Table 1)

The monthly resolution of the pCO_2 gridded data distributed throughout the study area satisfactorily represented the spatiotemporal variability; this was verified with the pCO_2 measurements available in the MP for the period analyzed. The specific gridded values in the coastal zone could present lower pCO_2 ranges since the averaging of several measurements would be underestimating the maximums recorded in the pCO_2 measurement, this point was discussed in the next section.

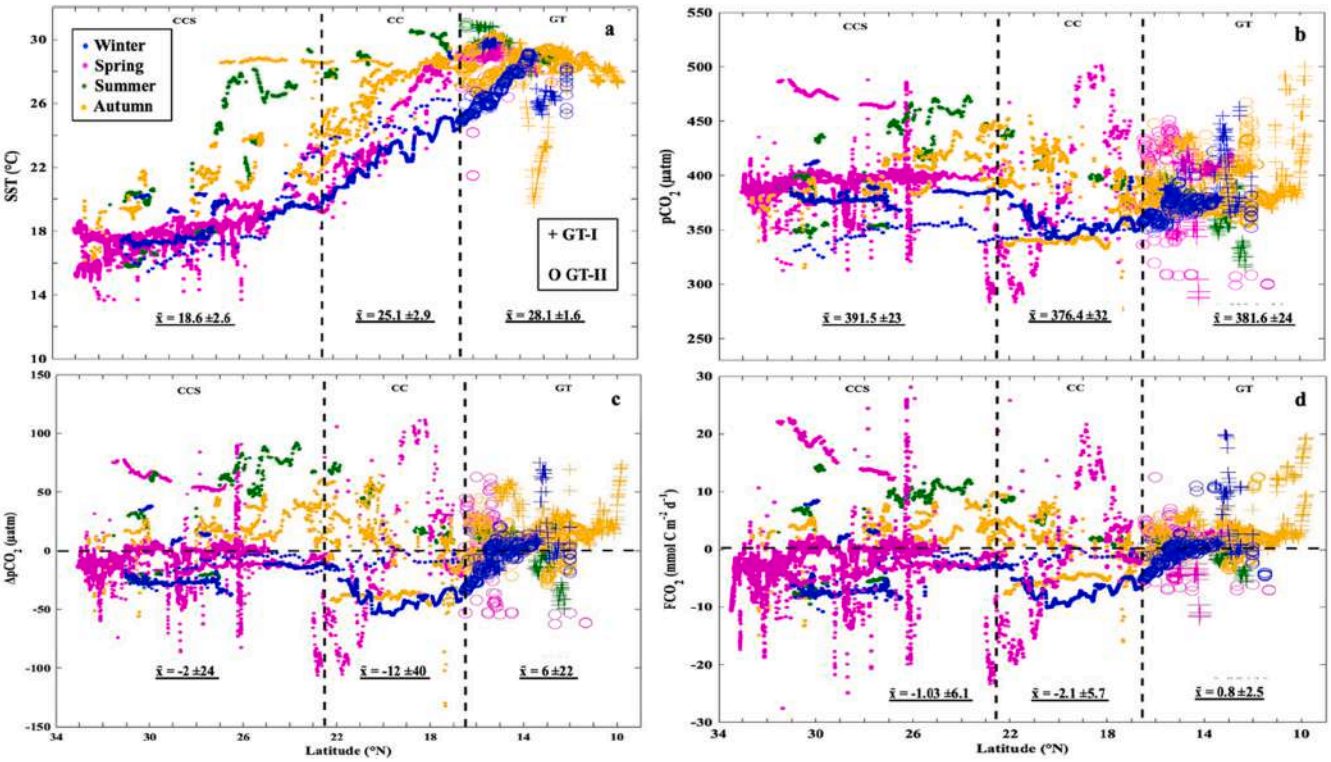

Fig. 2. Observed data of (a) sea surface temperature (SST), (b) partial pressure of CO_2 (pCO_2), and calculated data of (c) ΔpCO_2 and (d) ocean-atmosphere CO_2 fluxes (FCO_2). Colors indicate the season. Limits of the California Current System (CCS; 34–22.5° N), Cabo Corrientes (CC; 16.5–22.5° N), and Gulf of Tehuantepec (GT; 10–16.5° N) regions are indicated by the dashed lines. For the GT region, both areas are depicted by symbols (crosses: GT-I; circles: GT-II). The zero balance is indicated by a dashed horizontal black line (c, d). Average (± standard deviation) are also included for each region.

3.3. ΔpCO_2

Overall, calculated ΔpCO_2 values ranged from ∼ − 130 to 105 µatm throughout the study period (Fig. 2c). However, ΔpCO_2 presented a larger spatial variability (−132 to 105 µatm) within the CC region. CCS had values of −105 to 97 µatm, while GT exhibited a narrower ΔpCO_2 range (−58 and 88 µatm). The seasonal variability of ΔpCO_2 values varied among regions. Higher values were found in the spring in the CCS (97 µatm), CC (105 µatm), and autumn in the GT (87 µatm). In winter, below equilibrium, values were present in the CCS (−39 µatm), CC (−55 µatm), and GT-II (50 µatm). In the summer, the CCS (98 µatm) and CC (68 µatm) showed positive values, while the GT presented negative values (−50 µatm) and values near equilibrium (∼10 µatm). In the autumn, the CCS (55 µatm) and GT (88 µatm) regions showed positive values, although the CC presented negative values (−132 µatm) (Fig. 2c). In general, the seasonal average ΔpCO_2 values were higher in the CCS and CC regions in spring (30 ± 25 µatm and 36 ± 24 µatm, respectively; Table 1; Fig. 2c) and lower in GT-I (1 ± 32 µatm), with a maximum mean value observed in winter (61.4 ± 10 µatm) in this region. However, the minimum average value was found in winter in GT-II (−16 ± 13 µatm). Lastly, minimum mean values were present in winter in the CCS and CC (−15 ± 16 and − 32 ± 22 µatm, respectively).

Therefore, positive (negative) ΔpCO_2 values may help to infer what the FCO_2 to the atmosphere (ocean) would be like. However, the role played by wind is very important in the estimation of FCO_2 given its quadratic dependence on wind, and it may magnify the effect of sea-air exchanges.

3.4. FCO_2

Overall, the calculated FCO_2 values ranged between ∼ − 30 to 30 mmol C m^{-2} d^{-1} in the MP (Fig. 2d). Regarding spatial variability, the northern and central portions of the MP, corresponding to CCS and CC, had a greater dispersion of FCO_2 values, while the GT exhibited the least variability. FCO_2 values ranged from −27.6 to 29.8, −19.9 to 25.8, and − 11.7 to 20.8 mmol C m^{-2} d^{-1}, in the CCS, CC, and GT, respectively. In the GT, fluxes showed a narrower range with slightly positive and negative values, which contrasted with the CCS with large negative values (near ∼ − 30 mmol C m^{-2} d^{-1}); in GT the minimum values reached ∼ − 10 mmol C m^{-2} d^{-1}, whereas CC's spatial pattern suggests a transition condition between CCS and GT

On the other hand, seasonal variability in the CCS displayed the lowest seasonal mean flux estimated during winter (−4.3 ± 4.2 mmol C m^{-2} d^{-1}), while the highest average value was registered in spring (4.6 ± 4.2 mmol C m^{-2} d^{-1}; Table 1, Fig. 2d). CC presented the lowest mean FCO_2 in winter (−5.7 ± 3 mmol C m^{-2} d^{-1}), and the highest mean value during spring (4.2 ± 3 mmol C m^{-2} d^{-1}). Considering the segmentation of the GT, we observed that GT-II presented a seasonal mean FCO_2 of −1.8 ± 1.8 mmol C m^{-2} d^{-1} in winter and 1.3 ± 0.6 mmol C m^{-2} d^{-1} in summer; in GT-I, positive fluxes to the atmosphere were registered in winter of 8.9 ± 1.5 mmol C m^{-2} d^{-1}, with a minimum average in spring of 0.3 ± 3.6 mmol C m^{-2} d^{-1} (Table 1, Fig. 2d, SM4, SM6). In summer, there were no minimum or maximum values in any region, perhaps due to the scarcity of data at this time of year (SM1). It is important to highlight that the FCO_2 estimates from the pCO_2 measurements made in this study are consistent with the monthly gridded FCO_2 obtained from Valsala and Maksyutov (2010); that is, the range of values reported by these authors agrees with the values estimated in this work, both in magnitude and in the direction of flux. The gridded FCO_2 data used in the oceanic area adequately described the changes in the area in the different season. However, variations in the onshore may be imperceptible due to the resolution of the data (pixel size), which is discussed in the next section.

At the annual scale, the mean FCO_2 values for each region were ∼

−0.4, ∼ − 0.8, and ∼ 0.3 mol C m^{-2} $year^{-1}$ for the CCS, CC, and GT regions, respectively. Finally, when FCO_2 was integrated over the entire MP area (± standard deviation for whole data sets of the three regions), we found that ∼ − 10.9 ± 0.6 mol C m^{-2} had been absorbed by the ocean over the 25 years included in the study (SM9).

3.5. Stratification parameter

A latitudinal gradient in Φ was observed, with lower (higher) values in the north (south) (Fig. 3a, b). In the CCS, Φ values ranged between 200 and 500 J m^{-3}, the lowest in the MP, which suggests that reduced stratification in the water column due to a lower solar heating effect results in a shallower seasonal thermocline, and the highest pCO_2 values observed (Fig. 3b). Compared to that of the CCS, a higher Φ value (700 J m^{-3}) was observed in the CC. These two regions averaged Φ values far below those that have been previously reported, such as ∼1000 J m^{-3} in the CCS (Fiedler et al., 2013) and ∼ 1200 J m^{-3} in the CC (Franco et al., 2014). This was likely due to the data that were used here to estimate Φ being collected in winter and early spring. Although the range of our Φ values falls within those reported by Fiedler et al. (2013). Lastly, the highest Φ values (∼700 to ∼1100 J m^{-3}; Fig. 3a) were registered in the GT and suggested that the water column was well stratified, which resulted in lower pCO_2 values (Fig. 3b). However, during the Tehuano season, Φ decreased along with SST (SM2) while increasing pCO_2 values (Fig. 2b, SM5). Differences of up to ∼400 J m^{-3} in Φ values between GT-I and GT-II were observed, with noticeable larger values in GT-I reflecting the marked influence of vertical mixing induced by the intense winds.

3.6. Temperature-normalized pCO_2

The pCO_2 values normalized by temperature ($pCO_{2(norm)}$; Fig. 4a) allowed us to analyze pCO_2 without thermodynamic effects. This procedure allowed us to recognize that in Region I, in spring and summer, changes in pCO_2 are dominated by biological effects. Whereas in Region II pCO_2 remained small after removing the thermal effects, suggesting that biological effects play a minor role in the observed pCO_2 variability. Whereas, in Region II it remained constant when the thermodynamic effect was subtracted. In the case of the GT, only the GT-I zone is the one that presented greater variations during Tehuano's season, because the biological activity is a driver of change in pCO_2; this was not observed in the GT-II zone, where tropical conditions remained without significant

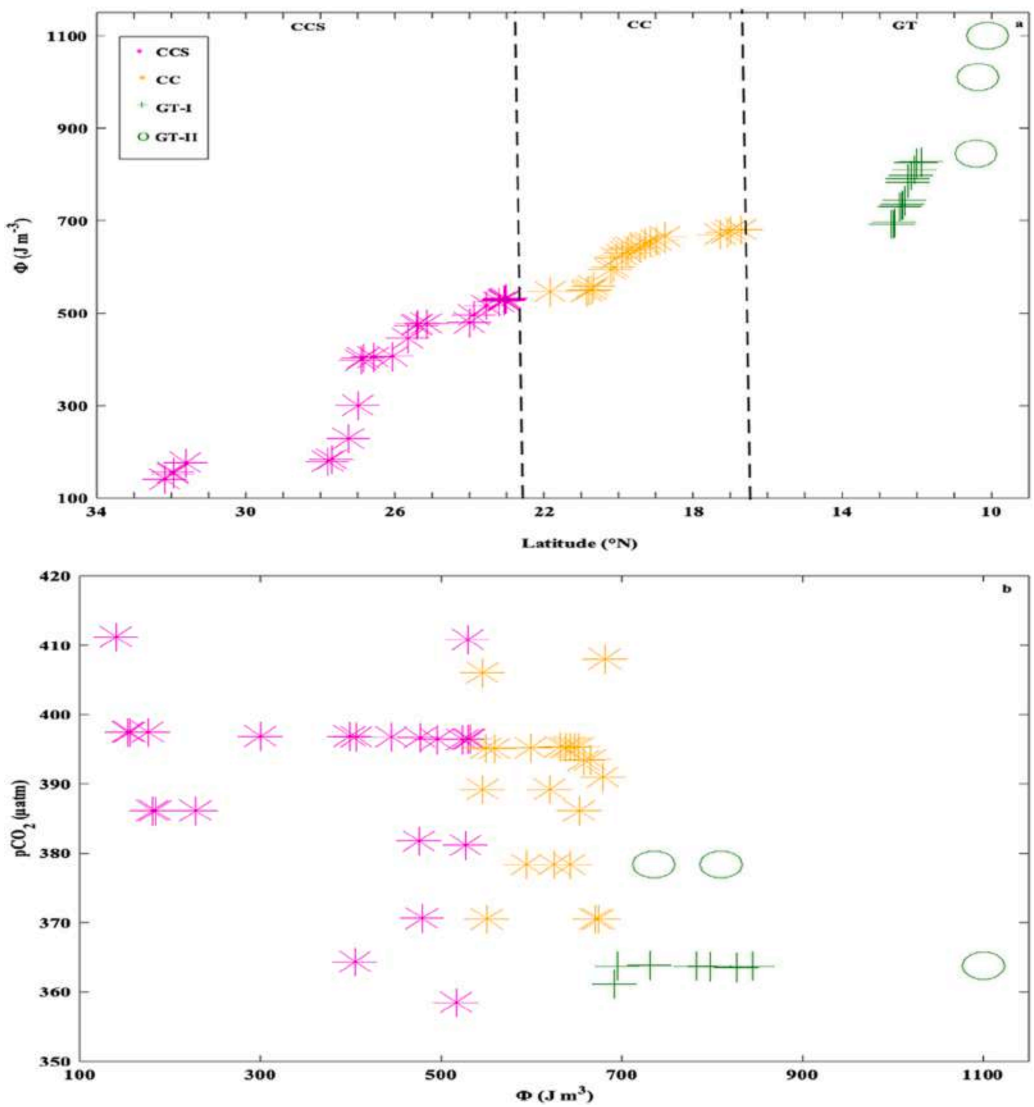

Fig. 3. (a) Latitudinal variation (by region) in the stratification parameter (Φ; J m^{-3}), and (b) values of Φ associated with pCO_2. The data used to estimate Φ come from World Ocean Database and correspond to the period of March–May (2005) (CCS), November–June (2005–2006) (CC), and October–November (2006) (GT).

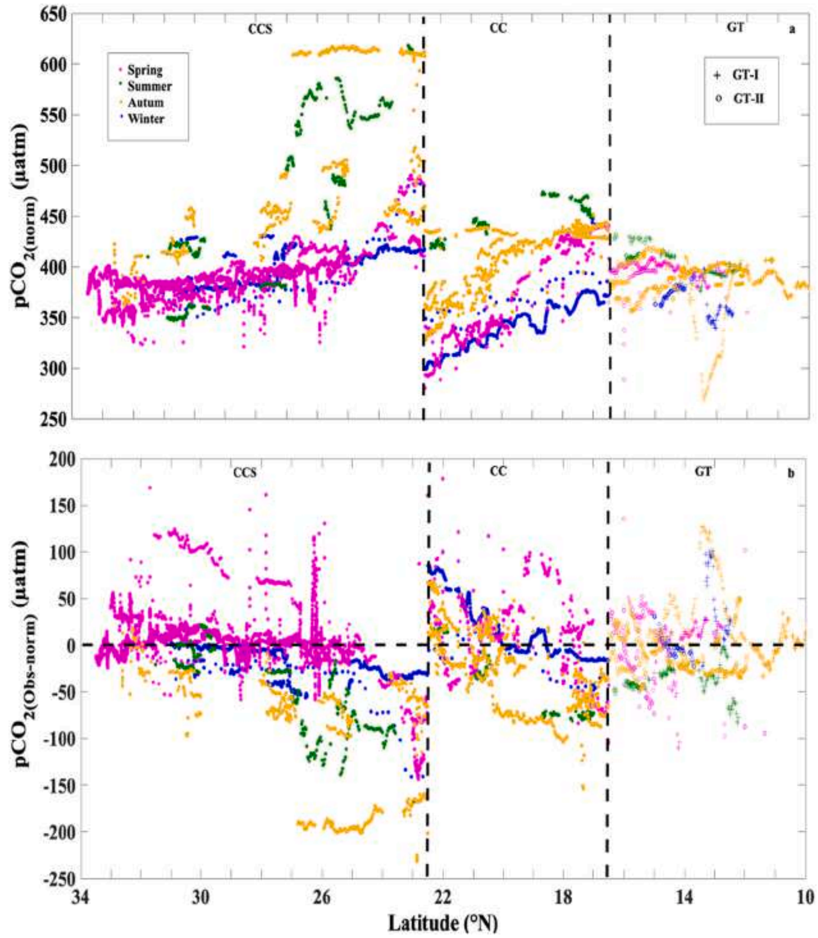

Fig. 4. (a) Temperature-normalized pCO_2 and (b) difference between observed pCO_2 (pCO_{2obs}) and normalized pCO_2 ($pCO_{2(norm)}$) values. The zero balance is indicated by a dashed horizontal black line. Vertical black dash lines indicate the limits of each region: the California Current System (CCS), Cabo Corrientes (CC), and Gulf of Tehuantepec (GT). The symbols + and o represent the values in the area of influence of Tehuanos (GT-I), and the area with tropical conditions (GT-II), respectively.

changes in pCO_2 values.

The difference between the pCO_2 values (pCO_{2obs}) and $pCO_{2(norm)}$ (Fig. 4b) was calculated. In the CCS, ~ 85% of the resulting values were positive during spring; while for 100% of the rest of the seasons, the values were negative. To CC and GT, around 60% of the resulting values were positive for all four seasons. Therefore, in autumn and winter in GT-I due to the influence of Tehuano winds, displace the water offshore from this warm-pool region, and the values. Thus, the thermodynamic effect was demonstrated in this case and in CCS during spring, where the temperature is the main driver of pCO_2. This result suggests that as global temperatures increase, the ocean capacity as a sink in this area will be reduced and thus the concentration of CO_2 in the atmosphere will increase.

3.7. Influence of ENSO events on carbon fluxes

During all periods of ENSO events, the FCO_2 values were positive, except in the El Niño event in 1994. The observed ENSO ranges of pCO_2 (~300 to ~470 µatm) and FCO_2 (−15 to ~20 mmol of C m^{-2} d^{-1}) decreased compared to those present under non-ENSO conditions (i.e., pCO_2 and FCO_2 ranges of 200 to 550 µatm and − 30 to 30 mmol C m^{-2} d^{-1}, respectively; Fig. 2d). Furthermore, the estimated FCO_2 integral value for the ENSO period was 7.8 mol C m^{-2}, and − 14.8 mol C m^{-2} for the non-ENSO. The mean FCO_2 values in ENSO conditions per region were ~ 5.7 ± 4.0, ~4.5 ± 3.7, and ~ 0.8 ± 2.4 mmol C m^{-2} d^{-1} for CCS, CC, and GT, correspondingly. These flux averages were different compared to non-ENSO means: CCS, CC, and GT exhibited FCO_2 of ~ −1.5 ± 6.0, ~ −2.9 ± 5.7, and ~ 0.9 ± 2.8 mmol C m^{-2} d^{-1}, respectively.

During the time frame of this study, three El Niño events (1994, 1997–1998, and 2015–2016) were recorded, which were classified as either moderate, strong, and very strong by the ONI index. During El Niño conditions, the SST had a maximum positive difference of ~3 °C with respect to climatology conditions in March. Under these conditions, pCO_2 and FCO_2 showed higher values, with 36 µatm and 9 mmol of C m^{-2} d^{-1}, respectively. However, SST registered lower values than the climatological means in September and October, with 1.2 and 2.1 °C, while pCO_2 showed smaller values in September but larger in October, −13 and 25 µatm, respectively. Likewise, FCO_2 values were larger under El Niño conditions in all cases, between 4 and 9 mmol of C m^{-2} d^{-1}.

Furthermore, each region showed distinct effects in both direct pCO_2 measurements and FCO_2 during El Niño events. The pCO_2 values in the CCS ranged from 320 to 460 µatm, while this variable ranged from 340 to 400 µatm in both the CC and GT regions (Fig. 5a). The average FCO_2 values (± standard deviation) during El Niño of 1994 by region were estimated to be ~ − 4.0 ± 3.2, ~2.2 ± 6.3, and ~ −3.1 ± 4.5 mmol C m^{-2} d^{-1} for the CCS, CC, and GT regions, respectively. Additionally, mean values were 6.4 ± 2.3, 4.9 ± 2.7, and 1.5 ± 0.2 mmol C m^{-2} d^{-1} for CCS, CC, and GT during El Niño 1998. Of particular interest, the average FCO_2 values were ~ 1.1 ± 0.8, ~1.4 ± 0.4, and ~ 9.6 ± 1.2

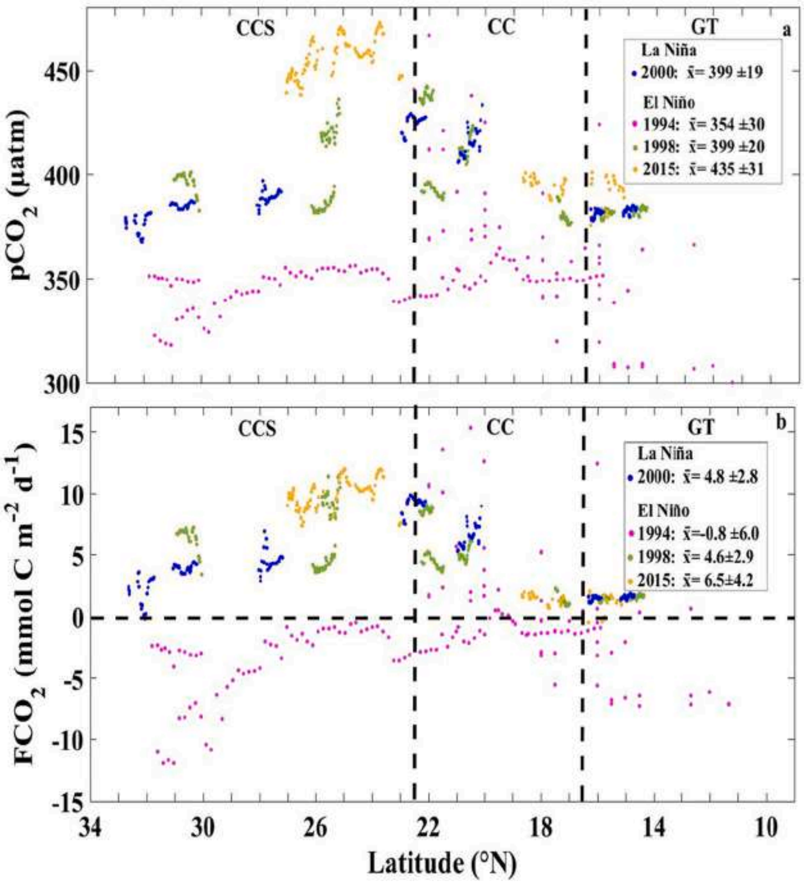

Fig. 5. Variations in (a) pCO_2 and (b) ocean-atmosphere CO_2 flux (FCO_2) during ENSO periods: El Niño 1994, 1997–1998, and 2015–2016 and La Niña 1998–2000. The zero balance is indicated by a dashed horizontal black line and shows equilibrium. The vertical black dash lines indicate the limits of each region: the California Current System (CCS), Cabo Corrientes (CC), and Gulf of Tehuantepec (GT). The numbers in the figure are the mean ± standard deviation of each event in the MP.

mmol C m^{-2} d^{-1} for the GT, CC, and CCS regions in El Niño 2015–2016. At an annual scale, FCO_2 mean values indicate a positive carbon flux (~1.7 mol C m^{-2} $year^{-1}$) in this same event. The interannual average variation of FCO_2 for the MP was ~4.0 mol C m^{-2} y^{-1} (SM8). Finally, the associated flux anomaly (calculated as the difference between the average fluxes during non-ENSO conditions and El Niño periods) showed a positive deviation of ~23 g C m^{-2} $year^{-1}$.

Data was only available for one La Niña event (1998–2000), which was classified as strong according to the ONI (Fig. 5a). During this event, the pCO_2 values ranged from 365 to 440 µatm, with higher values present in the north of the MP and lower values in the south. During this condition, SST decreased by up to 3 °C compared with the long-term mean, while pCO_2 and FCO_2 values were up to 15 µatm and 7 mmol C m^{-2} d^{-1}, respectively. The estimated average FCO_2 values were 1.5 ± 0.3, 5.5 ± 2.7, and 5.2 ± 2.5 mmol C m^{-2} d^{-1} in the GT, CC, and CCS regions, respectively (Fig. 5b). Area-integrated FCO_2 during this particular cold event was ~3.9 mol C m^{-2} for the entire MP (SM8).

Satellite monthly anomalies of SST_{sat}, ADT, and Chl_{sat} data from 2002 to 2018 were contrasted using Hovmöller diagrams for three transects: Baja California (33° N), Cabo Corrientes (20° N), and the Gulf of Tehuantepec (15° N; see Figs. 1 and 6). We selected these specific coastal areas because we wanted to illustrate the changes in SST_{sat}, ADT, and Chl_{sat} modulated by different processes in different regions of the MP, such as coastal upwelling and wind (e.g., Tehuanos' influence in the GT region). The influence of the El Niño/Blob 2014–2016 (Bond et al., 2015) with unusual increases in SST_{sat} and ADT was identified in the three transects, while negative Chl_{sat} anomalies dramatically decreased.

ADT anomalies exhibited interannual variations. For example, the lowest anomalies were recorded during La Niña in the three transects, (around −20 to −15 cm in the three sites). CCS presented negative anomalies ~10 cm; while CC and GT had the lowest values around −15 and − 20, respectively. El Blob/El Niño was also identified from mid-2015 to mid-2016, with maximum ADT anomalies of 15, 22, and 40 cm in CCS, CC, and GT, respectively (Figs. 6-8).

In general, during La Niña (El Niño) SST values were the lowest (highest) in these sites (Figs. 6 – 8); in cold conditions, the anomalies were up to −4.5 °C in CC and GT, and CCS had until −2.5 °C. While in the warm period the anomalies were 4° and 3 °C for CC – GT and CCS, respectively. Finally, in La Niña the chlorophyll-a concentration anomalies highest were in CCS and CC (2 and 7 mg m^{-3}, respectively), and in GT greatest anomalies values were 2 mg m^{-3} for this condition. During El Niño conditions Chl_{sat} anomalies were up to 7 mg m^{-3} in CC; while CCS and GT had 2 mg m^{-3} in this period (Figs. 6–8).

3.8. Statistical analyses

Although the distribution of pCO_2 data throughout the study area suggested a heterogeneous pattern along regions, they presented statistical differences in both in-situ data and satellite information (i.e., SST, ADT, and Chl). Statistical analyses were conducted with the medians of the SST_{sat}, SST_{insitu}, ADT, pCO_2, and FCO_2, as the data were highly scattered around the mean. The results of the Bayesian *t*-tests for the five variables indicated that all sets of values, by region and season, had a high probability (> 90%) of the medians being different. The exception was in CC and GT in the summer, when we found that the probability dropped to 50% (with 95% credibility intervals) among all

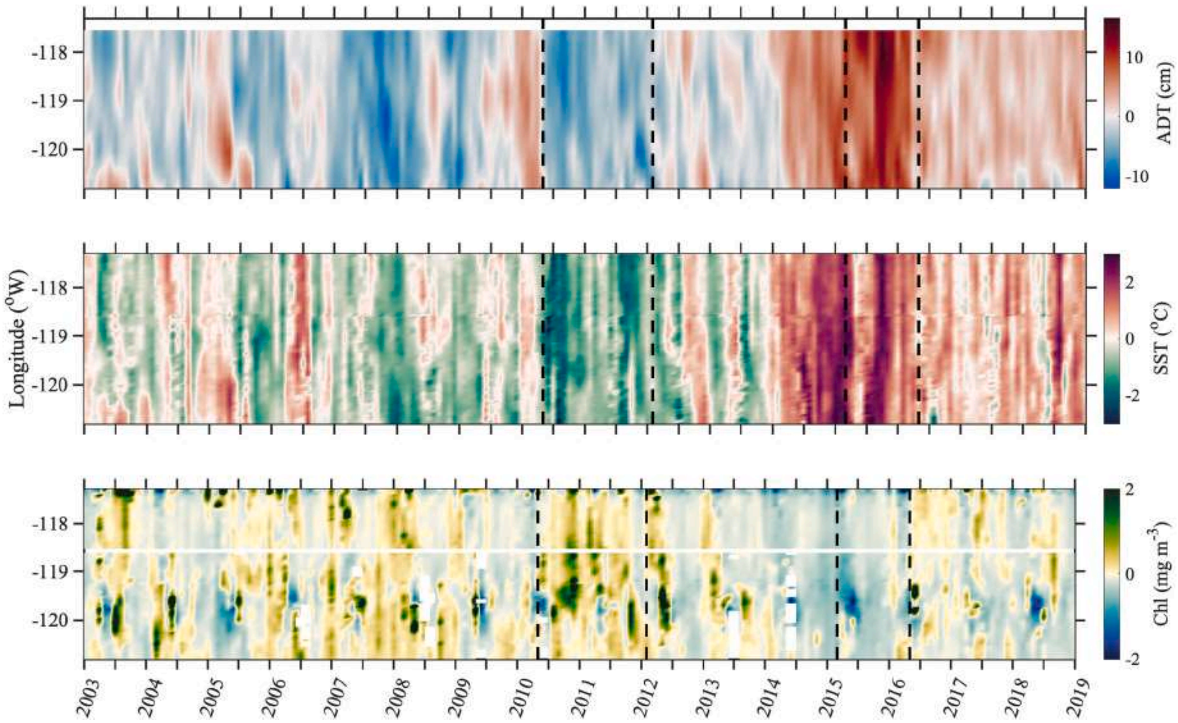

Fig. 6. Time evolution of anomalies from an onshore-offshore transect at 33° N (California Current System, CCS). Monthly anomalies of (a) Absolute dynamic topography (ADT, cm), (b) sea surface temperature (SST_{sat}, °C), and (c) chlorophyll-a (Chl_{sat}, mg m^{-3}). Values are referred to as the long-term (2003–2018) monthly climatological mean. Vertical dash lines indicate the La Niña (2010−2012) and El Niño (2015–2016) conditions.

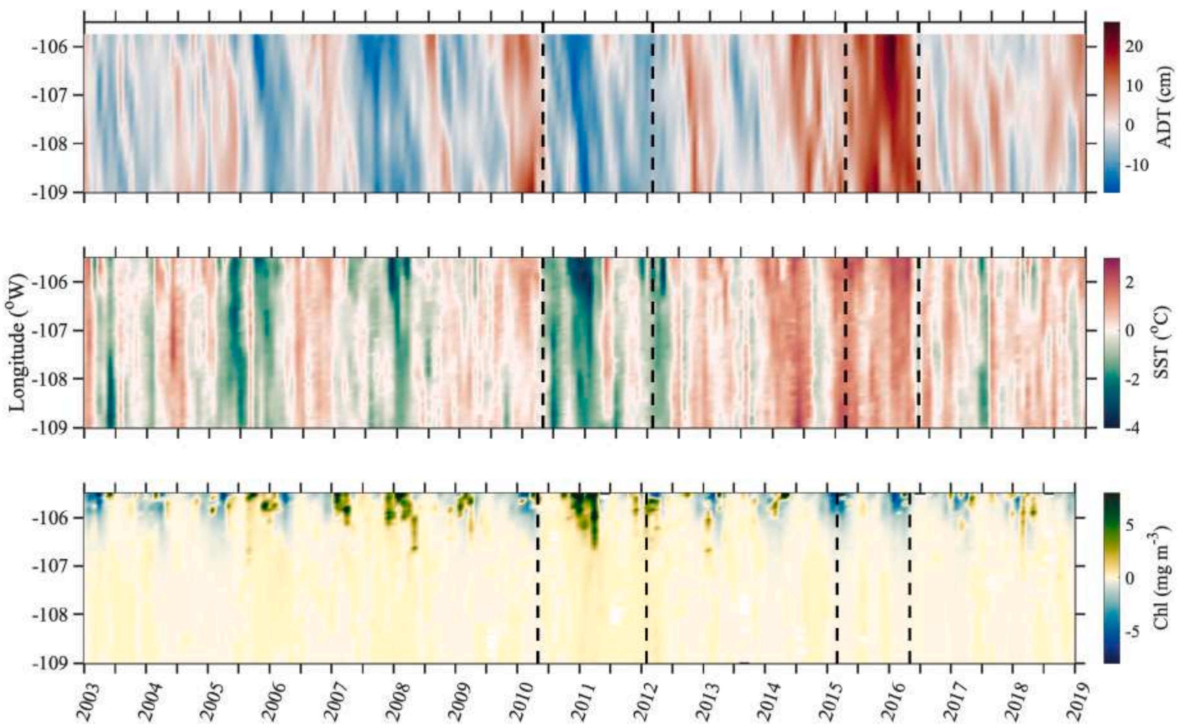

Fig. 7. As in Fig. 6 but for transect at 20° N (Cabo Corrientes, CC).

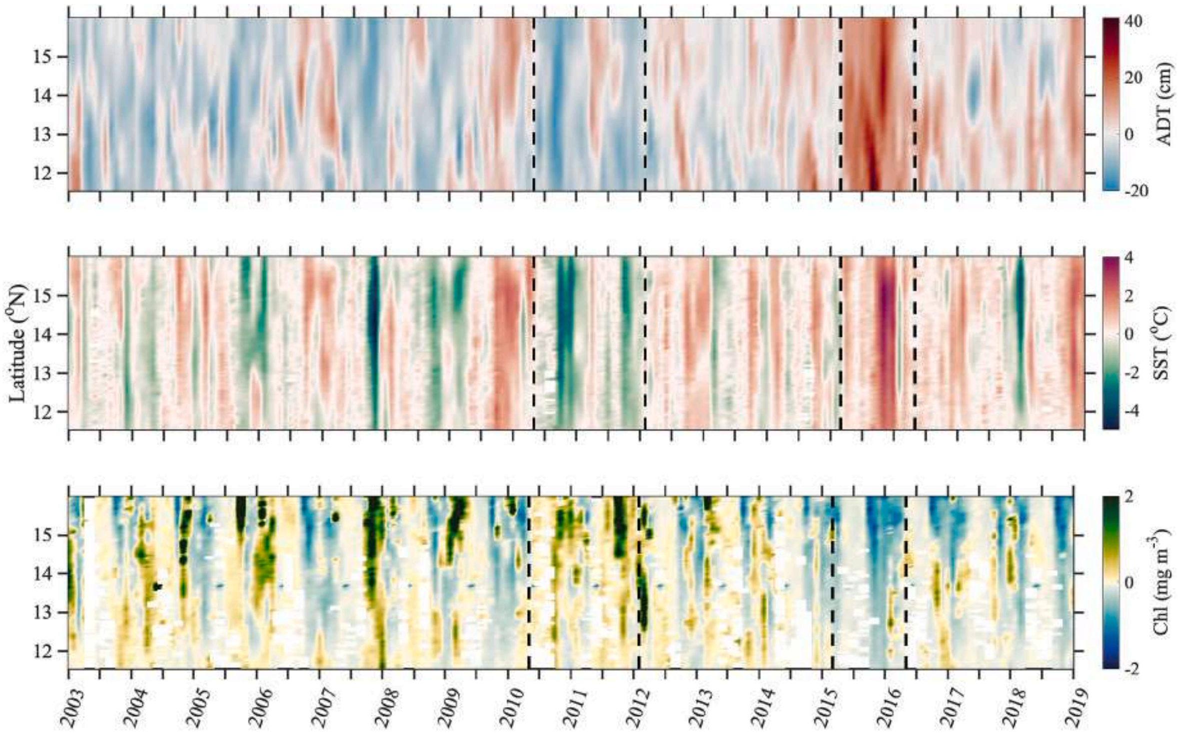

Fig. 8. As in Fig. 6 but for transect at 15° N (Gulf of Tehuantepec, GT).

variables

4. Discussion

4.1. MP regionalization

While the Mexican Pacific subdivision has been analyzed from a physical oceanography perspective (Durazo and Baumgartner, 2002; Flores-Morales et al., 2009; Fiedler et al., 2013), our study has shown that the chemical conditions of the MP may also be used to consistently subdivide the MP into the three proposed geographic areas at any time of the year. The identification of the main physical processes in each region that modulate the chemical oceanographic conditions allowed us to discern which are the forcing agents that characterized them: a) in the CCS, seasonal upwelling; b) in CC, being a transition area of commingling water masses, with the presence of tropical water and upwelling in a specific area (around 20° N); and c) in GT, where the wind is the driver that allowed us to subdivide into two subregions. However, despite being a chemical regionalization (based purely on pCO_2, and FCO_2), it is important to note that chemical parameters are modulated directly by the physical dynamics (SST, ADT), as was substantiated by the statistical results.

The results of Φ suggest that increased surface water heating at lower latitudes acts as a barrier to water-column mixing. At higher values of Φ, more energy is required for mixing and the transport of subsurface water to the surface. The highest Φ values were present in the southern areas of each region. Therefore, the CCS region presented greater mixing ease due to its low Φ values (Fig. 3a), whereas the GT region showed greater stratification (Fig. 3a) and high ADT values (SM3) and anomalies (~20 cm; Fig. 8) during the non-Tehuano season. The GT is located within an OMZ, and during the Tehuano season (autumn and winter), the water in GT-I that reaches the surface has lower temperatures (SM2), high concentrations of dissolved inorganic carbon, high total alkalinity, and low oxygen values. In GT-II, the Φ values were maintained relatively high (Fig. 3a; Fiedler and Lavín, 2016; Chapa-Balcorta et al., 2015).

When evaluating the estimates of Φ (Fig. 3a), it is necessary to highlight that subsurface water reaches the surface in the CC and GT regions when water-column stratification is weakened by either upwelling or Tehuano-wind conditions. During these seasonal events, the surface water is enriched with high levels of pCO_2 (Chapa-Balcorta et al., 2015; Coronado-Álvarez et al., 2017), which implies that these regions act as sources of CO_2 to the atmosphere. However, for the GT, each scenario presented an exception. This is, in autumn and winter, the influence of Tehuano winds resulted in low Φ values due to vertical mixing (i.e., GT-I), but these winds also produce two convergence conditions to the north and south of the area influenced by Tehuano winds (Fiedler and Lavín, 2016; Chapa-Balcorta et al., 2015). Both areas under this convergence condition showed higher Φ values than the area in which the Tehuano winds were present.

This suggests that GT-I (e.g., the area directly influenced by Tehuano winds) is a CO_2 source (on average) in autumn and winter. During spring and summer, the mean FCO_2 value was near equilibrium (0.3 ± 3.6 and 0.7 ± 2.0 mmol C m^{-2} d^{-1}, respectively). During autumn and winter, GT-II behaved (on average) as a source and sink, correspondingly. Nevertheless, variability was lost when these variables were averaged for the whole GT region. This has two implications. Firstly, as expected this region alternates its role as a CO_2 source and sink (Takahashi et al., 2009; Walker Brown et al., 2015). Thus, the same region can emit or absorb CO_2, depending on the time of year and the reigning conditions (e.g., El Niño events or strong northerly winds). Secondly, the upward transport of CO_2-rich water to the surface under upwelling conditions initially turns the area into a CO_2 source; however, this is counteracted by a greater biological effect due to elevated nutrient concentrations, which promotes the uptake of carbon species (Lluch-Cota et al., 1997). In the 25 years of data included in this study, it was found that during winter the GT-I region acts as a source of CO_2 while GT-II acts as a sink in this season, whereas the CCS and CC regions act as sources during spring.

4.2. pCO_2 regionalization

The range of pCO_2 values was similar in the three regions, although the CCS resulted in the highest mean of whole data sets (gridded and measurements) (Fig. 2). In autumn and winter, the GT-I presented maximum values due to Tehuano winds, while the CC region acted as a tropical-subtropical transition zone dependent on the confluence of two large oceanic currents: the equatorward California Current and near-surface poleward Mexican Coastal Current (Kessler, 2006; Godínez et al., 2010). This pattern may be explained by the seasonal oceanographic conditions of each region.

The study regions, i.e., CCS and CC, present seasonal coastal upwelling (from March to September and to May, respectively), with 15 days upwelling period (intensification – relaxation; Coronado-Álvarez et al., 2017), which results in increased primary productivity during the relaxation of these conditions (around five days after the intensification). This promotes greater CO_2 fixation in the ocean (inducing a reduction in pCO_2 levels), although the initial intensification of these events results in the emission of CO_2 to the atmosphere (Coronado-Álvarez et al., 2017). However, it is necessary to further the understanding of the effects of Tehuano winds at high-frequency time scales to discern changes in the carbon system during different periods, in addition to evaluating the changes in the seasonal enrichment of the GT in their chemical implications vg., pCO_2 and FCO_2 fluctuations.

In addition, in the CCS region, the surface waters are colder due to the influence of Sub-Arctic Water (Durazo and Baumgartner, 2002), while surface waters from the CC and GT regions are warm and of tropical origin (Fiedler and Lavín, 2016). If we only take into account the thermodynamic factor and its influence on pCO_2 in the latitudinal gradient, thus it is possible to state that gas solubility is greater in water with low temperatures as can be observed in waters of higher latitudes (Sabine et al., 2004). This implies that the CC and GT regions have lower abilities to absorb atmospheric CO_2 compared to the CCS region.

In our regionalization, we used gridded and measurement data. It is important to mention that we found that the gridded pCO_2 data represent temporal changes; however, when short periods are analyzed, the detail of spatial-temporal oscillations caused by different drivers is lost, e.g., physical and biological: upwelling and Tehuanos winds, and blooms, respectively, among others. This fact has implications when analyzing gridded data because it emphasizes the need to understand the dynamics of each study area, and to have measurements that provide an overview of the changes in pCO_2 over time. The use of measurements and gridded data was analyzed in the special subheading in this section.

4.3. Ocean-atmosphere CO_2 dynamics

There have been reports that pCO_2 and FCO_2 variability is lower in oceanic areas, while in coastal regions these could be underestimated (Takahashi et al., 2009). Several studies have established that the MP is a source of CO_2 to the atmosphere (Chavez et al., 2007), or an area near equilibrium (Zhang and Tian, 2019; DiNezio et al., 2015). Also, these kinds of studies have assumed that the MP has homogeneous oceanographic features and carbon fluxes resulting in the whole MP as a source of this gas. In contrast, our study found that the MP showed high geographical and seasonal heterogeneity within each region. This suggests that the general assumption that this area is a net source of CO_2 must be reconsidered. Our results have established that: 1) regionalization based on physical features also corresponded with chemical conditions (i.e., pCO_2 and FCO_2), 2) Seasonal variations in FCO_2 in each area occur with different magnitudes, suggesting that the impacts of SST and local atmospheric forcings (such as Tehuano winds and upwelling events) vary seasonally. This is especially true for CCS and CC physical seasonal processes, such as upwellings (that occur in spring), that increase FCO_2 variability (Coronado-Álvarez et al., 2017; Franco et al., 2014). In GT-I, the FCO_2 values are high in autumn-winter because Tehuano winds cause upwelling that brings high-pCO_2 subsurface water to the surface. However, GT-II alternated its role as a source and sink of CO_2 among seasons. Therefore, the wind plays an important role in both water-column mixing and FCO_2 estimations, as suggested by Coronado-Álvarez et al. (2017). 3) The results of this study raise new questions that address these subjects from different perspectives (e.g., FCO_2 trends during different periods, flux variations associated with biological activity, and the impacts of climatic phenomena on the sea-air exchange of CO_2 at different spatial-temporal scales). Regarding the seasonal FCO_2 variability in the GT, new questions have been raised that need to be investigated such as Tehuano and non-Tehuano conditions, and the high-frequency variability to identify the drivers that impact pCO_2 changes.

On average, GT-I acts as a source during Tehuano conditions; the water that rises to the surface has high pCO_2 values and low levels of oxygen. It should be noted that the MP is located within one of the largest oxygen minimum zones on the planet (Paulmier and Ruíz-Pino, 2009) where denitrification processes also occur (Thomas, 1966). Therefore, it is necessary to understand how biological conditions are affected by chemical changes in the ocean in this region. For example, it is expected that upwelled waters in the area would have low pH values due to ocean acidification (Caldeira and Wickett, 2003), which causes harmful effects on calcifying organisms. This has a series of repercussions on the ecosystem, such as the loss of biodiversity and impacts on fisheries and, therefore, socio-economic impacts.

4.4. ENSO conditions

The occurrence of ENSO events modifies oceanographic dynamics. For example, during El Niño conditions, a decrease in the intensity of trade winds in the eastern Pacific yields reduced precipitation and biological activity, while SST increases (Rasmusson and Carpenter, 1982). The opposite is observed under La Niña conditions.

As described by Franco et al. (2014), in situ data anomalies in this work suggest that during warm months, the SST in La Niña conditions is lower (~ -1.0 °C) due to seasonal masking, while temperature anomalies of up to 3 °C were observed during the El Niño. Likewise, satellite data (Figs. 6 – 8) showed SST anomalies up to −5 °C in GT, and around −3 and − 4 °C in CCS and CC during La Niña (2010−2011). Despite El Niño/Blob, the SST anomaly was between 3 and 4 °C. Also, ADT anomalies (Figs. 6 – 8) were observed, with positive (negative) values during El Niño (La Niña). This illustrates the impact, which differed in magnitude, of these warm (cold) conditions. These results showed that the wind intensity is reduced, causing ADT monthly anomalies to be higher, resulting in thermocline sinking, which leads to low Chl_{sat} monthly anomalies (Figs. 6 - 8).

Studies that contrast the effects of El Niño in the ocean and the effects that occur over various spatial-temporal scales are needed (Chatterjee et al., 2017), particularly since CO_2 emissions from the ocean to the atmosphere are reduced by around 40–60% when ENSO conditions are present. Park et al. (2010) estimated a high negative correlation between El Niño and FCO_2, indicating that the ocean acts as a CO_2 sink under these conditions. Chavez et al. (1999) and Feely et al. (1999, 2002, 2006) also indicated that during El Niño conditions, FCO_2 is seaward. This means that according to the largest estimations about FCO_2 during El Niño conditions, FCO_2 must reduce (in some cases is negative) and temperature increase; however, our results showed that the temperature increased while the FCO_2 values were positive, varying degrees for each region, this flux was positive (around 4 to 9 mmol m^{-2} d^{-1}. This suggests that the impact of El Niño in the MP varies depending on the particular geographic area being considered, as well as the season in which ENSO conditions occur (Franco et al., 2014), and highlights the likely influence of local oceanographic features (Trucco-Pignata et al., 2019).

The FCO_2 values during the El Niño/Blob decreased in magnitude, although with fluxes towards the atmosphere. In addition, Chat anomalies indicated that photosynthetic activity was reduced, varying its value in each transect, as the results indicated negative values in the most intense El Niño/Blob period (2015–2016) (from 2 to 7 mg m^{-3}; Figs. 6 -8). This supports the conclusion that the degree of interannual variations differed depending on the region. On the contrary, greater CO_2 fixation through photosynthesis that favored a reduction in the flow of CO_2 to the atmosphere was observed under La Niña conditions (Chiodi et al., 2014; Coronado-Álvarez et al., 2017). This last point was corroborated with Chl_{insitu} data (not shown) for the La Niña of 1998–2000, during which the highest recorded values were present in the CCS (~13.8 mg m^{-3}; De La Cruz-Orozco et al., 2010) and GT (4.5 mg m^{-3}) regions. Moreover, we estimated FCO_2 anomalies for this cold period, and its values were higher, up to 7 mmol C m^{-2} d^{-1} to the atmosphere. Also, with satellite data anomalies of chlorophyll, we observed that during La Niña (2010–2012), in the three transects the Chl_{sat} were the highest (among 2 and 7 mg m^{-3}; Figs. 6 – 8). This suggests that in these cold periods the ocean is a source and at the same time it has high primary productivity, using chlorophyll as a proxy for it. During this condition, the extension of California Current Water (CCW) can be found between southern Cabo San Lucas and the CC region due to the intensification of winds and an increase in southward surface advection (Baumgartner and Christensen Jr., 1985; Portela et al., 2016). Jones et al. (2001, their Figure 9b) found FCO_2 anomalies under La Niña conditions that ranged between 3 and 15 g C m^{-2} $year^{-1}$. Based on our calculations, the estimated anomaly under La Niña conditions was ~29 g C m^{-2} $year^{-1}$, which was consistent with what was reported by Jones et al. (2001), as it was positive, although of a different magnitude.

Even though more information is needed, these differences could in part be associated with two concepts. First, it is possible that the local physical dynamics of each region dominate the effects of ENSO events, resulting in interannual signals that are concealed, as noted by Franco et al. (2014) and Durazo et al. (2017) for the CC and CCS regions, respectively. That is, the impact of a cold (warm) event during a warm (cold) season will likely be clearly exposed. It is perhaps for this reason that our results were different among the three regions in this study. The periods in which the ENSO events occurred and their interactions with the conditions of each region may have resulted in these differences. For example, for the El Niño of 1994, the pCO_2 and FCO_2 values were lower than those of the 1997–1998 and 2015–2016 El Niño events. This is primarily because the El Niño of 1994 was classified as moderate according to the ONI, while those of 2015–2016 and 1997–1998 were classified as some of the strongest events ever recorded (Bond et al., 2015; https://ggweather.com/enso/oni.htm). However, there is a lack of data during the period in which the El Niño of 1997–1998 had the greatest influence to fully substantiate the statement. Second, these differences could in part be associated with the precipitation ranges, which oscillate seasonally. For example, in the CCS, a direct relationship between the ENSO multivariate index (MEI) and precipitation occurs. This could be associated with a greater anomalous presence of Tropical Surface Water during the El Niño conditions of 2015–2016, as described by Trucco-Pignata et al. (2019). However, from the CC region to lower latitudes, the relationship is inverted (Bravo-Cabrera et al., 2017). Thus, the magnitude of FCO_2 varied in each event, suggesting that the impact of ENSO conditions will fluctuate depending on both: the geographic area and the season in which it occurs, and also, the seasonal oceanographic conditions of a particular region.

Therefore, our study showed that the proposed regionalization based on chemical dynamics responds to the physical oceanographic conditions in the MP. Likewise, the spatio-temporal changes such as season and ENSO conditions of the analyzed variables (e.g., SST, pCO_2, FCO_2) were identified. Also, we observed that the MP is a CO_2 sink that fluctuates seasonally in each region. This has not been described in detail in a time series as long as the one studied in this work. However, further efforts are required to identify the drivers influencing pCO_2 through time, with high-frequency resolutions. Additionally, there is a need to analyze more data in the GT region to identify the changes in the region under Tehuano and non-Tehuano conditions, and their chemical and biological implications. It remains necessary to explore other factors that may be at work to understand how physical, chemical, and biological processes must be taken into consideration to determine how they are modified by ENSO events in both time and space.

The sea absorbs about 30% of the CO_2 emitted into the atmosphere (Sabine et al., 2004), the increase in atmospheric CO_2 is followed by the ocean, which increased pCO_2 to ~1.5 μatm per year (Cai et al., 2020). Therefore, the equilibrium conditions between the sea and the air increase over time, and in turn the ocean's capacity to absorb this gas decreases. In the case of MP, in the 25 years of study, it was observed that in warm conditions the pCO_2 of the sea is higher than the atmospheric pCO_2. Therefore, it is assumed that an increase in sea temperature in MP would cause positive ΔpCO_2, although it is necessary to analyze long-term trends in SST.

4.5. *Implications of the use of measured and gridded data*

One of the implications of working with thousands of data of different kinds (measured and gridded), as in this work, is that when integrating it, it is important to ensure that the latter are consistent with the spatiotemporal variation of the variables studied, pCO_2 and FCO_2. Therefore, it was decided to take a sample of the measured versus gridded data and compare the magnitude of the values with measurements. To cite an example: the gridded pCO_2 value of ~361 μatm (16° N 107.5° W) was similar to measurements by Nojiri (2014) ~376 μatm (~16° N ~ 108° W) (data that we used in both cases). Our findings were consistent and strengthen what was mentioned by Takahashi et al. (2014), the gridded products are means resulting from pCO_2 measurements reported decades ago (Takahashi et al., 2013). This was consistent with Takahashi et al. (2014), who mentioned that the pCO_2 gridded values are lower because they were the result of the average of many measurements. The pCO_2 gridded values were taken offshore of the MP, it is considered that the spatiotemporal changes adequately describe the variability of the zone, according to Pennington et al. (2010), because the area has low variability, as discussed below. Our findings suggest that gridded pCO_2 represented the changes in MP offshore. And therefore, the identification of small changes in pCO_2 onshore may be difficult to identify.

On other hand, Franco et al. (2014) reported FCO_2 close to equilibrium (~ < −1 mmol m^{-2} d^{-1}) at Cabo Corrientes (20° N, 105° W) in November 2009; our gridded results showed a CO_2 flux of ~ − 1.05 mmol m^{-2} d^{-1}, for that point in the same month in 2014. Although the magnitudes of the fluxes were similar in this case, it should be noted that this gridded product always presents lower values than the measurements due to the very nature of being average calculations. However, the similarities of our results may be because the gridded FCO_2 was calculated with a coefficient (Wanninkhof, 1992), whose results are 20% higher in magnitude (Wanninkhof, 2014), concerning the one used in the estimations we made (Wanninkhof, 2014). Perhaps this difference was compensated by the underestimation and therefore the values were similar, this issue needs to be verified. Therefore, we can affirm that the gridded data represent variations in MP in time and space; however, the values of these variables could be subestimated at lower spatiotemporal scales of lower resolutions and not detect local processes. Thus, this must be considered when making use of gridded data.

These gridded products are considered useful as a proxy for the existing variation generally over time; however, in coastal areas, they have their limitations as mentioned above. With the spatial resolution they have (1 × 1° or others of 5 × 4°; Takahashi et al. (2013), Valsala and Maksyutov (2010), respectively) processes such as upwelling, advection, Tehuanos that affect the FCO_2 in temporal scales of days and smaller spatial their signals decrease or disappear, v.g. the Tehuanos zone, the upwelling season located at Baja California Peninsula; whose geographical areas are smaller concerning the whole MP. Therefore, the onshore, the gridded products lose details of processes that affect both pCO_2 and FCO_2; while at a larger spatial scale and offshore, they adequately represent the changes over time of these variables. This is because the greatest variability in pCO_2 and FCO_2 has been reported in the first ~50 km from the coastline to the open ocean, at greater distances over time, this variation decreases oscillating at or near equilibrium values, as reported by Pennington et al. (2010). Although these findings were made for a transect of the California Current upwelling system, the coast-ocean dynamics are similar; the range of FCO_2 and pCO_2 values will depend on the processes prevailing in any particular coastal area (Laruelle et al., 2014).

We observed that FCO_2 coincides in direction and in many cases in magnitude as mentioned in the Cabo Corrientes area. However, there are differences between estimated and gridded values, with a variance of $\sim$1.1 mol m^{-2} d^{-1}. This value was obtained from the maximum variance (0.4 mol m^{-2} y^{-1}) shown by Valsala and Maksyutov (2010) (see Fig. 5 of these authors); who did not report the FCO_2 estimation error or uncertainty in their gridded data. The latter is crucial to provide, as it allows us to interpret the data appropriately. Another relevant issue is that gridded FCO_2 was estimated based on Wanninkhof (1992) coefficients while our FCO_2 estimates are based on Wanninkhof (2014), which are about 20% higher. Future comparisons should consider standardizing the gridded FCO_2.

Another important aspect to mention in our work is that we use a reanalysis of wind data (Kalnay et al., 1996). The calculation of the gas transfer coefficient (k, see Eq. 1) with a reanalysis of wind data was within the reported ranges (Wanninkhof, 2014). Therefore, this type of product for FCO_2 estimation is considered adequate (Kisler et al., 2001), but also provides a more robust flux estimate than a single interpolation method based on a single wind product (Dong et al., 2022).

Finally, this implies that, as mentioned above, gridded data provide a general idea of the spatiotemporal conditions of pCO_2 and FCO_2, although they underestimate the measured values, especially in the nearshore whose dynamics affect these variables. Also, provide the uncertainty or error of the measurements and estimates for greater reliability of the use of this data. Therefore, our results are valid in order to categorize and describe the three proposed regions; it is essential to have pCO_2 and FCO_2 measurements that support the gridded information and provide us with elements to understand the impact of the drivers in the coastal zone.

5. Conclusions

The results of the statistical analyses indicated that the three regions presented high probabilities of being different from each other. With these results, it was possible to strengthen the regionalization of the MP with both physical and chemical variables.

The FCO_2 values during the 25 years of data included in this study by season, region of the MP, and year, showed high probabilities of being different between areas and seasons. Fluxes were different between regions in terms of magnitude and direction. For example, in spring, the ocean in the three regions acted as a source of CO_2 but to varying degrees. In summer, the CCS and CC regions acted as sinks, while GT-I acted as a source in autumn and winter. In the same seasons, GT-II acted as a source and sink. Overall, it was estimated that the MP has acted as a CO_2 sink (−10.9 mol C m^{-2}). Nonetheless, the MP presented variations by region, indicating that the CCS and CC are net sinks of CO_2, while the GT is a net source of CO_2 to the atmosphere.

The use of different sources of pCO_2 and FCO_2 data with different products (measured and gridded) and integrating them to describe their spatiotemporal variation and discuss the drivers that affect them, represents a great challenge that was addressed in this work. It can be concluded that 1) in order to adequately describe changes across space (onshore - offshore), frequent measurements over time are required in order to identify the processes that affect them. 2) The coastal area is the zone with the greatest temporal and spatial variation of pCO_2 and FCO_2; the variations in the seaward are small. 3) The gridded products provide a very close idea of the temporal changes in the oceanic area; however, in the near shore, the spatial resolution has limitations since the identification of processes occurring in that area is lost. Both products, pCO_2, and FCO_2 gridded values are subestimated the magnitude of measurements, around 10 μatm, and 1.1 mmol m^{-2} d^{-1}, respectively.

Finally, it was identified that the impact of ENSO conditions was different in each region, which caused the FCO_2 to vary depending on the season and the area of the MP (SM9). We found also that El Niño conditions caused both positive and negative FCO_2, while during La Niña it was reported as a source of this gas.

Declaration of Competing Interest

None.

Data availability

See method section. We explain were the data base is coming from.

Acknowledgements

The first author was supported by a grant from Consejo Nacional de Ciencia y Tecnología (CONACyT) for a postdoctoral stay at the Instituto de Investigaciones Oceanológicas (IIO) of the Universidad Autónoma de Baja California (UABC). This work was partially supported by Desarrollo De Un Sensor Submarinos De pH y Temperatura De Bajo Costo Con Aplicaciones A Estudios De La Acidificacion En Zonas Acuicolas En B·C (Convocatoria Interna 22th- UABC). LEC received

Researcher Performance Incentives (EDI), and Committee on Operation and Promotion of Academic Activities (COFAA) scholarships from the Instituto Politécnico Nacional.

Appendix A. Supplementary data

Supplementary data to this article can be found online at https://doi.org/10.1016/j.jmarsys.2022.103853.

References

Bakker, D.C.E., Pfeil, B., Smith, K., Hankin, S., Olsen, A., Alin, S.R., Cosca, C., Harasawa, S., Kozyr, A., Nojiri, Y., O'Brien, K.M., Schuster, U., Telszewski, M., Tilbrook, B., Wada, C., Akl, J., Barbero, L., Bates, N.R., Boutin, J., Bozec, J., Cai, W. J., Castle, R.D., Chavez, F.P., Chen, L., Chierici, M., Currie, K., de Baar, H.J.W., Evans, W., Feely, R.A., Fransson, A., Gao, Z., Hales, B., Hardman-Mountford, N.J., Hoppema, M., Huang, W.J., Hunt, C.W., Huss, B., Ichikawa, T., Johannessen, T., Jones, E.M., Jones, S.D., Jutterström, S., Kitidis, V., Körtzinger, A., Landschützer, P., Lauvset, S.K., Lefèvre, N., Manke, A.B., Mathis, J.T., Merlivat, L., Metzl, N., Murata, A., Newberger, T., Omar, A.M., Ono, O., Park, G.H., Paterson, K., Pierrot, D., Ríos, A.F., Sabine, C.L., Saito, S., Salisbury, J., Sarma, V.V.S.S., Schlitzer, R., Sieger, R., Skjelvan, I., Steinhoff, T., Sullivan, K.F., Sun, H., Sutton, A.J., Suzuki, T., Sweeney, C., Takahashi, T., Tjiputra, J., Tsurushima, N., van Heuven, S.M.A., Vandemark, D., Vlahos, P., Wallace, D.W.R., Wanninkhof, R., Watson, A.J., 2014. An update to the surface ocean CO_2 atlas (SOCAT version 2). Earth Syst. Sci. Data 6, 69–90. https://doi.org/10.5194/essd-6-69-2014.

Bakker, D.C.E., Pfeil, B., Landa, C.S., Metzl, N., O'Brien, K.M., Olsen, A., Smith, K., Cosca, C., Harasawa, S., Jones, S.D., Nakaoka, S., Nojiri, Y., Schuster, U., Steinhoff, T., Sweeney, C., Takahashi, T., Tilbrook, B., Wada, C., Wanninkhof, R., Alin, S.R., Balestrini, C.F., Barbero, L., Bates, N.R., Bianchi, A.A., Bonou, F., Boutin, J., Bozec, Y., Burger, E.F., Cai, W., Castle, R.D., Chen, L., Chierici, M., Currie, K., Evans, W., Featherstone, C., Feely, R.A., Fransson, A., Goyet, C., Greenwood, N., Gregor, L., Hankin, S., Hardman-Mountford, N.J., Harlay, J., Hauck, J., Hoppema, M., Humphreys, M.P., Hunt, C.W., Huss, B., Ibánhez, J.S.P., Johannessen, T., Keeling, R., Kitidis, V., Körtzinger, A., Kozyr, A., Krasakopoulou, E., Kuwata, A., Landschützer, P., Lauvset, S.K., Lefèvre, N., Lo Monaco, C., Manke, A., Mathis, J.T., Merlivat, L., Millero, F.J., Monteiro, P.M.S., Munro, D.R., Murata, A., Newberger, T., Omar, A.M., Ono, T., Paterson, K., Pearce, D., Pierrot, D., Robbins, L. L., Saito, S., Salisbury, J., Schlitzer, R., Schneider, B., Schweitzer, R., Sieger, R., Skjelvan, I., Sullivan, K.F., Sutherland, S.C., Sutton, A.J., Tadokoro, K., Telszewski, M., Tuma, M., van Heuven, S.M.A.C., Vandemark, D., Ward, B., Watson, A.J., Xu, S., 2016. A multi-decade record of high-quality fCO_2 data in version 3 of the Surface Ocean CO_2 atlas (SOCAT). Earth Syst. Sci. Data 8, 383–413. https://doi.org/10.5194/essd-8-383-2016.

Baumgartner, T., Christensen Jr., N., 1985. Coupling of the Gulf of California to large-scale interannual climatic variability. J. Mar. Res. 4, 825–848. https://doi.org/10.1357/002224085788453967.

Bond, N.A., Cronin, M.F., Freeland, H., Mantua, N., 2015. Causes and impacts of the 2014 warm anomaly in the NE Pacific. Geophys. Res. Lett. 42, 3414–3420. https://doi.org/10.1002/2015GL063306.

Boyer, T.P., Baranova, O.K., Coleman, C., García, H.E., Grodsky, A., Locarnini, R.A., Mishonov, A.V., Paver, C.R., Reagan, J.R., Seidov, D., Smolyar, I.V., Weathers, K.W., Zheng, M.M., 2018. In: Mishonov, A.V. (Ed.), World Ocean Database 2018. NOAA Atlas NESDEIS, p. 87. https://www.ncei.noaa.gov/access/world-ocean-database/datawodgeo.html. Accessed January 2021.

Bravo-Cabrera, J.L., Azpra-Romero, E., Zarraluqui-Such, V., Gay-García, C., 2017. Effects of El Niño in Mexico during rainy and dry seasons: an extended treatment. Atmósfera 30, 221–232. https://doi.org/10.20937/ATM.2017.30.03.03.

Cai, WJ., Xu, YY., Feely, R.A., et al., 2020. Controls on surface water carbonate chemistry along North American ocean margins. Nat Commun 11, 2691. https://doi.org/10.1038/s41467-020-16530-z.

Caldeira, K., Wickett, M., 2003. Anthropogenic carbon and ocean pH. Nature 425, 365. https://doi.org/10.1038/425365a.

Cepeda-Morales, J., Gaxiola-Castro, G., Beier, E., Godínez, V.M., 2013. The mechanisms involved in defining the northern boundary of the shallow oxygen minimum zone in the eastern tropical Pacific Ocean of Mexico. Deep Res. Part I Oceanogr. Res. Pap. 76, 1–12. https://doi.org/10.1016/j.dsr.2013.02.004.

Chapa-Balcorta, C., Hernández-Ayón, J.M., Durazo, R., Beier, E., Alin, S.R., López-Pérez, A., 2015. Influence of post-tehuano oceanographic processes in the dynamics of the CO_2 system in the Gulf of Tehuantepec, Mexico. J. Geophys. Res. Ocean. 120, 7752–7770. https://doi.org/10.1002/2015JC011249.

Chapa-Balcorta, C., Sosa-Ávalos, R., Hernández-Ayón, J.M., Espinosa-Carreón, T.L., Lara-Lara, J.R., Guerra-Mendoza, R., 2019. Almacenes y flujos en ecosistemas marinos. In: Paz-Pellat, F., Hernández-Ayón, J.M., Sosa-Ávalos, R., Velázquez-Rodríguez, A.S. (Eds.), Estado del Ciclo del Carbono: Agenda Azul y Verde. Programa Mexicano del Carbono, Texcoco, Estado de México, México, pp. 3–23.

Chatterjee, A., Gierach, M., Sutton, A., Feely, R., Crisp, D., Eldering, A., Gunson, M., O'Dell W, Stephens B, and Schimel D., 2017. Influence of El Niño on atmospheric CO_2 over the tropical Pacific Ocean: findings from NASA'S OCO-2 mission. Science 358, 6360. https://doi.org/10.1126/science.aam5776.

Chavez, F.P., Strutton, P.G., Friederich, G.E., Feely, R.A., Feldman, G.C., Foley, D.G., McPhaden, M.J., 1999. Biological and chemical response of the equatorial Pacific Ocean to the 1997–98 El Niño. Science 286, 2126–2131. https://doi.org/10.1126/science.286.5447.2126.

Chavez, F.P., Takahashi, T., Cai, W.J., Friederich, G., Hales, B., Wanninkhof, R., Feely, R. A., 2007. Coastal Oceans. In: King, A.W., Dilling, L., Zimmerman, G.P., Fairman, D. M., Houghton, R.A., Marland, G., Rose, A.Z., Wilbanks, T.J. (Eds.), The First State of the Carbon Cycle Report (SOCCR): The North American Carbon Budget and Implications for the Global Carbon Cycle. A Report by the US Climate Change Science Program and the Subcommittee on Global Change Research. National Oceanic and Atmospheric Administration, National Climatic Data Center, Asheville, NC, pp. 149–156.

Chiodi, A.M., Dune, J.P., Harrison, D.E., 2014. Comment on Qian et al. 2008: La Niña and El Niño composites of atmospheric CO_2 change. Tellus Ser. B Chem. Phys. Meteorol. 66 (1), 20428. https://doi.org/10.3402/tellusb.v66.20428.

Chiodi, A.M., Dune, J.P., Harrison, D.E., 2019. Estimating air-sea carbon flux uncertainty over the tropical Pacific: importance of winds and wind analysis uncertainty. Glob. Biogeochem. Cycles 33, 370–390. https://doi.org/10.1029/2018GB006047.

CMEMS, 2020. Absolute Dynamic Topography. SEALEVEL_GLO_PHY_MDT_008_063. https://doi.org/10.48670/moi-00150.

Coronado-Álvarez, L.L.A., Álvarez-Borrego, S., Lara-Lara, J.R., Solana-Arellano, E., Hernández-Ayón, J.M., Zirino, A., 2017. Temporal variations of water pCO_2 and the air–water CO_2 flux at a coastal location in the southern California current system: diurnal to interanual scales. Ciencias Marinas 43, 137–156. https://doi.org/10.7773/cm.v43i3.2707.

De La Cruz-Orozco, M.E., Valdez-Holguín, J.E., Gaxiola-Castro, G., Mariano-Matías, M., Espinosa-Carreón, T.L., 2010. Flujos de CO_2 océano–atmósfera. In: Gaxiola-Castro, G., Durazo, R. (Eds.), Dinámica del ecosistema pelágico frente a Baja California 1997–2007. SEMARNAT, INE, CICESE, UABC, México, DF, pp. 165–179.

DeGrandpe, M., Hammar, T., Wirick, C., 1998. Short-term pCO_2 and O_2 dynamics in California coastal waters. Deep-Sea Res. II 45, 1557–1575. https://doi.org/10.1016/S0967-0645(98)80006-4.

DiNezio, P.N., Barbero, L., Long, M., Lovesnduski, N., Deser, C., 2015. Are anthropogenic changes in the tropical ocean carbon cycle masked by Pacific decadal variability? US Clivar Variat. 13, 12–16.

Dong, Y., Bakker, D., Bell, T., Huang, B., Landschützer, P., Liss, P., Yang, M., 2022. Update on the temperature corrections of global Air-Sea CO2 flux estimates. Global Biog. Cyc 36, 1–13. https://doi.org/10.1029/2022GB007360.

Durazo, R., 2015. Seasonality of the transitional region of the California current system off Baja California. J. Geophys. Res. Oceans 120, 1173–1196. https://doi.org/10.1002/2014JC010405.

Durazo, R., Baumgartner, T., 2002. Evolution of oceanographic conditions off Baja California: 1997-1999. Prog. Oceanogr. 54, 7–31. https://doi.org/10.1016/S0079-6611(02)00041-1.

Durazo, R., Baumgartner, T., Bograd, S.J., Collins, C.A., De la Campa, S., García, J., Gaxiola, G., Huyer, A., Hyrenbach, D., Loya, D., Lynn, R.J., Schwing, F.B., Smith, R. L., Sydeman, W.J., Wheeler, P., 2001. The state of the California current 200-2001: a third straight La Niña year. In: CalCOFI Reports, 42, pp. 29–60.

Durazo, R., Castro, R., Miranda, L.E., Delgadillo-Hinojosa, F., Mejía-Trejo, A., 2017. Anomalous hydrographic conditions off the northwestern coast of the Baja California peninsula during 2013–2016. Cien. Mar. 43, 81–9281. https://doi.org/10.7773/cm.v43i2.2754.

Falkowski, P., Scholes, R.J., Boyle, E., Canadell, J., Canfield, D., Elser, J., Gruber, N., Hibbard, K., Högberg, P., Linder, S., Mackenzie, F.T., Morel, I.I.I., Pedersen, T., Rosenthal, Y., Seitzinger, S., Smetacek, V., Steffen, W., 2000. The global carbon cycle: A test of our knowledge of earth as A system. Science 290, 291–296. https://doi.org/10.2307/3078125.

Feely, R.A., Lamb, M.F., Greeley, D.J., Wanninkhof, R., 1999. Comparison of the carbon system parameters at the global CO_2 survey crossover locations in the North and South Pacific Ocean, 1990–1996. In: ORNL/CDIAC- 115. Carbon Dioxide Inf. Anal. Cent., Oak Ridge Natl. Lab., U.S. Dep. of Energy, Oak Ridge, Tenn. Estados Unidos de América. https://doi.org/10.2172/1157069, 74 pp.

Feely, R., Sabine, C.L., Lee, K., Millero, F.J., Lamb, M.F., Greeley, D., Bullister, J.L., Key, R.M., Peng, T.H., Kozyr, A., Ono, T., Wong, S., 2002. In situ calcium carbonate dissolution in the Pacific Ocean. Blobal Biochem. Cycles 16, 902–912. https://doi.org/10.1029/2002GB001866.

Feely, R.A., Sabine, C.L., Byrne, R.H., Greeley, D., 2006. Direct evidence for ocean acidification of the North Pacific Ocean. In: EOS Transactions of the American Geophysical Union 87, Fall Meeting Supplement, Abstract OS12B-04.

Fiedler, P.C., Lavín, M., 2016. Oceanographic conditions of the eastern tropical Pacific. In: Glynn, P.W., et al. (Eds.), Coral Reefs of the Eastern Tropical Pacific, Coral Reefs Of The World, 8. https://doi.org/10.1007/978-94-017-7499-4_3.

Fiedler, P.C., Mendelssohn, R., Palacios, D.M., Bograd, S.J., 2013. Pycnocline variations in the eastern tropical and North Pacific, 1958–2008. J. Clim. 26, 583–599. https://doi.org/10.1175/JCLI-D-11-00728.1.

Flores-Morales, A.L., Parés-Sierra, A., Marinone, S.G., 2009. Factors that modulate the seasonal variability of the sea surface temperature in the eastern tropical Pacific. Geofis. Int. 48, 337–349.

Franco, A.C., Hernández-Ayón, J.M., Beier, E., Garçon, V., Maske, H., Paulmier, A., Färber-Lorda, J., Castro, R., Sosa-Ávalos, R., 2014. Air-sea CO_2 fluxes above the stratified oxygen mínimum zone in the coastal region of Mexico. J. Geophys. Res. Ocean. 119, 1–15. https://doi.org/10.1002/2013JC009337.

Friederich, G., Ledesma, J., Ulloa, O., Chavez, F.P., 2008. Air–sea carbon dioxide fluxes in the coastal southeastern tropical Pacific. Prog. Oceanogr. 79, 156–166. https://doi.org/10.1016/j.pocean.2008.10.001x.

Friedlingstein, P., Jones, M.W., O'Sullivan, M., Andrew, R.M., Bakker, D.C.E., Hauck, J., Le Quéré, C., Peters, G.P., Peters, W., Pongratz, J., Sitch, S., Canadell, J.G., Ciais, P., Jackson, R.B., Alin, S.R., Anthoni, P., Bates, N.R., Becker, M., Bellouin, N., Bopp, L., Chau, T.T.T., Chevallier, F., Chini, L.P., Cronin, M., Currie, K.I., Decharme, B., Djeutchouang, L., Dou, X., Evans, W., Feely, R.A., Feng, L., Gasser, T., Gilfillan, D., Gkritzalis, T., Grassi, G., Gregor, L., Gruber, N., Gürses, Ö., Harris, I., Houghton, R. A., Hurtt, G.C., Iida, Y., Ilyina, T., Luijkx, I.T., Jain, A.K., Jones, S.D., Kato, E., Kennedy, D., Klein Goldewijk, K., Knauer, J., Korsbakken, J.I., Körtzinger, A., Landschützer, P., Lauvset, S.K., Lefèvre, N., Lienert, S., Liu, J., Marland, G., McGuire, P.C., Melton, J.R., Munro, D.R., Nabel, J.E.M.S., Nakaoka, S.-I., Niwa, Y., Ono, T., Pierrot, D., Poulter, B., Rehder, G., Resplandy, L., Robertson, E., Rödenbeck, C., Rosan, T.M., Schwinger, J., Schwingshackl, C., Séférian, R., Sutton, A.J., Sweeney, C., Tanhua, T., Tans, P.P., Tian, H., Tilbrook, B., Tubiello, F., van der Werf, G., Vuichard, N., Wada, C., Wanninkhof, R., Watson, A., Willis, D., Wiltshire, A.J., Yuan, W., Yue, C., Yue, X., Zaehle, S., Zeng, J., 2021. Global Carbon Budget 2021, Earth Syst. Sci. Data discuss. [preprint]. https://doi.org/10.5194/essd-2021-386 in review.

Godínez, V.M., Beier, E., Lavín, M.F., Kurczyn, J.A., 2010. Circulation at the entrance of the Gulf of California from satellite altimeter and hydrographic observations. J. Geophys. Res. 115, C04007. https://doi.org/10.1029/2009JC005705.

Hales, B., Struton, P., Saraceno, M., Letelier, R., Takahashi, T., Feely, R., Sabine, C., Chavez, F., 2012. Satellite-based prediction of pCO_2 in coastal waters of eastern North Pacific. Prog. Oceanogr. 103, 1–15. https://doi.org/10.1016/j.pocean.2012.03.001.

Held, L., Sabanés, Bové D., 2014. Applied Statistical Inference: Likelihood and Bayes. Springer, Heidelberg (376 pages, ISBN: 3642378862).

Hernández-Ayón, J.M., Gaxiola-Castro, G., Chavez, F., Takahashi, T., Feely, D., Sabine, C. L., Hales, B., Lara-Lara, J.R., 2010. Variabilidad espacial y temporal del flujo de CO_2 océano-atmósfera. In: Gaxiola-Castro, G., Durazo, R. (Eds.), Dinámica del ecosistema pelágico frente a Baja California 1997–2007. SEMARNAT, INE, CICESE, UABC, México, DF, pp. 197–208.

Jones, C., Collins, M., Cox, P., Spall, S., 2001. The carbon cycle response to ENSO: A coupled climate-carbon cycle model study. J. Clim. 14, 4113–4129. https://doi.org/10.1175/1520-442(2001)0142.0.CO;2.

Kalnay, E., Kanamitsu, M., Kistler, R., Collins, W., Deaven, D., Gandin, L., Iredell, M., Saha, S., White, G., Woollen, J., Zhu, Y., Chelliah, M., Ebisuzaki, W., Higgins, W., Janowiak, J., Mo, K.C., Ropelewski, C., Wang, J., Leetmaa, A., Reynolds, R., Jenne, R., Joseph, D., 1996. The NCEP/NCAR 40-year reanalysis project. Bull. Amer. Meteor. Soc. 77, 437–470. https://doi.org/10.1175/1520-0477(1996)077<0437:TNYRP>2.0.CO;2.

Kelter, R., 2020. Bayesian alternatives to null hypothesis significance testing in biomedical research: a non-technical introduction to Bayesian inference with JASP. BMC Med. Res. Methodol. 20, 142. https://doi.org/10.1186/s12874-020-00980-6. PMID: 32503439; PMCID: PMC72753119.

Kessler, W.S., 2006. The circulation of the eastern tropical Pacific: A review. Prog. Oceanogr. 69, 181–217.

Kisler, R., Kalnay, E., Collinas, W., Saha, S., White, G., Woollen, J., Chelliah, M., Ebisuzaki, W., Kanamitsu, M., Kousky, V., van den Dool, H., Jenne, R., Fiorino, M., 2001. The NCEP-NCAR 50-year Reanalyses monthly means CD-ROM and documentation. Bull. Am. Meteorol. Soc. 2, 247–268. https://doi.org/10.1175/1520-0477(2001)082<0247:TNNYRM>2.3.CO;2.

Kruschke, J.K., 2013. Bayesian estimation supersedes the t test. J. Exp. Psychol. General 142, 573–603.

Laruelle, G.G., Lauerwald, R., Pfeil, B., Regnier, P., 2014. Regionalized global budget of the CO_2 exchange at the air–water interface in continental shelf seas. Global Biogeochem Cy. 28, 1199–1214. https://doi.org/10.1002/2014GB004832.

Lauvset, S.K., Lange, N., Tanhua, T., Bittig, H.C., Olsen, A.C., Kozyr, A., Álvarez, M., Becker, S., Brown, P.J., Carter, B.R., Cotrim da Cunha, L., Feely, R.A., van Heuven, S., Hoppema, M., Ishii, M., Jeansson, E., Jutterström, S., Jones, S.D., Karlsen, M.K., Lo Monaco, C., Michaelis, P., Murata, A., Pérez, F.F., Pfeil, B., Schirnick, C., Steinfeldt, R., Suzuki, T., Tilbrook, B., Velo, A., Wanninkhof, R., Woosley, R.J., Key, R.M., 2021. An updated version of the global interior ocean biogeochemical data product, GLODAPv2.2021. Earth Syst. Sci. Data Discuss. 1–32. https://doi.org/10.5194/essd-2021-234.

Liss, P., Merlivat, L., 1986. Air-Sea exchange rates: introduction and synthesis. In: Buart Menard, P. (Ed.), The Role of Air-Sea Exchange in Geochemical Cycling. Reidel Publishing Company, Boston, pp. 113–127.

Lluch-Cota, S., Álvarez-Borrego, S., Santamaría-Del-Ángel, E., Müller-Karger, F., Hernández-Vázquez, S., 1997. The Gulf of Tehuantepec and adjacent areas: spatial and temporal variation of satellite-derived phtotosynthetic pigments. Ciencias Marinas 23, 329–340. https://doi.org/10.7773/cm.v23i3.809.

Lynn, R., Simpson, J., 1987. The California current system: the seasonal variability of its physical characteristics. J. Geophys. Res. 92, 947–966. https://doi.org/10.1029/JC092iC12p12947.

Mariano-Matías, M., Gaxiola-Castro, G., De La Cruz Orozco, M.E., Chavez, F.P., 2016. Seasonal air–sea CO_2 fluxes in the southern California current off the Baja California peninsula (Mexico). Cienc. Mar. 42, 157–177. https://doi.org/10.7773/cm.v42i3.2651.

Muñoz-Anderson, M., Lara-Lara, J.R., Álvarez-Borrego, S., Bazán-Guzmán, C., De la Cruz-Orozco, M., 2015. Water–air carbon fluxes in the coastal upwelling zone off northern Baja California. Cien. Mar. 41, 157–168. https://doi.org/10.7773/cm.v41i2.2484.

Nakaoka, S., Telszewski, M., Nojiri, Y., Yasunaka, S., Miyazaki, C., Mukai, H., Usui, N., 2013. Estimating temporal and spatial variation of ocean surface pCO_2 in the North Pacific using a self-organizing map neural network technique. Biogeosciences 10, 6093–6106. https://doi.org/10.5194/bg-10-6093-2013.

NASA, 2021a. Goddard Space Flight Center, Ocean Ecology Laboratory, Ocean Biology Processing Group. Moderate-Resolution Imaging Spectroradiometer (MODIS) Aqua (Daily Sea Surface Temperature 4 Km Data). NASA Ob. DAAC, Greenbelt, MD, USA. https://doi.org/10.5067/MODSA1D4D4. Accessed on 25/01/2021.

NASA, 2021b. Goddard Space Flight Center, Ocean Ecology Laboratory, Ocean Biology Processing Group. Moderate-Resolution Imaging Spectroradiometer (MODIS) Aqua (Daily Chlorophyll 4 Km Data.) NASA Ob. DAAC, Greenbelt, MD, USA. https://doi.org/10.5067/AQUA/MODIS/LM3/CHL/2018. Accessed on 25/01/2021.

NOAA, 2018. Ocean Acidification Data Stewardship (OADS). https://www.ncei.noaa.gov/access/oads/. Consulted December 2021.

Nojiri, Yukihiro, 2014. Documentation of CO_2 Measurements during PYXIS Cruise PX108W. https://doi.org/10.1594/PANGAEA.813903.

Park, G., Wanninkhof, R., Doney, S., Takahashi, T., Lee, K., Feely, R., Sabine, C., Triñanes, J., Lima, I., 2010. Variability of global net sea-air CO_2 fluxes over the las three decades using empirical relationships. Tellus 62, 352–368. https://doi.org/10.1111/j.1600-0889.2010.00498.x.

Paulmier, A., Ruíz-Pino, D., 2009. Oxygen minimum zones (OMZs) in the modern ocean. Prog. Ocen. 80, 113–128. https://doi.org/10.1016/j.pocean.2008.08.001.

Pennington, J., Castro, C., Collins, C., Evans, W., Friederich, G., Michisaki, R., Chavez, F., 2010. The northern and Central California coastal upwelling system. In: Liu, K., Atkinson, L., Quiñones, R., Talaue McMaus, L. (Eds.), Carbon and Nutrient Fluxes in Continental Margins Global Change. Springer, Berlin, pp. 29–44.

Portela, E., Beier, E., Barton, E., Castro, R., Godínez, V., Palacios-Hernández, E., Fiedler, P., Sánchez-Velasco, L., Trasviña, A., 2016. Water masses and circulation in the tropical Pacific off Central Mexico and surrounding areas. Amer. Met. Soc. 46, 3069–3081. https://doi.org/10.1175/JPO-D-16-0068.1.

Rasmusson, E., Carpenter, T., 1982. Variations in tropical se surface temperature and surface winds Associeted with the southern oscillation /El Niño. Mon. Weather Rev. 110, 354–384. https://doi.org/10.1175/1520-0493(1982)110<0354:VITSST>2.0.CO;2.

Reid, P., Fischer, A., Lewis-Brown, E., Meredith, M., Sparrow, M., Andersson, A., Antia, A., Bates, N., Bathmann, U., Beaugrand, G., Brix, H., Dye, S., Edwars, M., Furevik, T., Gangst, R., Hatún, H., Hopcroft, R., Kendall, M., Kasten, S., Keeling, R., Le-Queré, C., Mackenzie, F., Malin, G., Mauritzen, C., Olafsson, J., Paull, C., Rignot, E., Shimada, K., Vogt, M., Wallace, C., Wang, Z., Washington, R., 2009. Impacts of the oceans on climate change. Ad. Mar. Biol 56, 1–150. https://doi.org/10.1016/S0065-2881(09)56001-4.

Sabine, C.L., Feely, R., Gruber, N., Key, R., Lee, K., Bullister, J., Wanninkhof, R., Wong, C., Wallace, D., Tilbrook, B., Millero, F., Peng, T., Kozyr, A., Ono, T., Rios, A., 2004. The oceanic sink for anthropogenic CO_2. Science 305, 367–371. https://doi.org/10.1126/science.1097403.

Simpson, J.H., 1981. The shelf-sea fronts: implications of their existence and behavior. Phil. Trans. R. Soc. Lond. A 302, 531–546. https://doi.org/10.1098/rsta.1981.0181.

Soppa, M.A., Peeken, I., Bracher, A., 2017. Global chlorophyll-a concentrations for diatoms, haptophytes and prokaryotes obtained with the diagnostic pigment analysis of HPLC data compiled from several databases and individual cruises. PANGAEA. https://doi.org/10.1594/PANGAEA.875879.

Sutton, A.J., Wanninkhof, R., Sabine, C.L., Feely, R.A., Cronin, M.F., Weller, R.A., 2017. Variability and trends in surface seawater pCO_2 and CO_2 flux in the Pacific Ocean. Geophys. Res. Lett. 44, 5627–5636. https://doi.org/10.1002/2017GL073814.

Takahashi, T., Sutherland, S.C., Wanninkhof, R., Sweeney, C., Feely, R.A., Chipman, D. W., Hales, B., Friederich, G., Chavez, F., Sabine, C., Watson, A., Bakker, D., Schuster, U., Metzl, N., Yoshikawa-Inoue, H., Ishii, M., Midorikawa, T., Nojiri, Y., Kortzinger, A., Steinhoff, T., Hoppema, M., Olafsson, J., Arnarson, T., Tilbrook, B., Johannessen, T., Olsen, A., Bellerby, R., Wong, C., Delille, B., Bates, N.R., de Baar, H. J.W., 2009. Climatological mean and decadal change in surface ocean pCO_2, and net sea–air CO_2 flux over the global oceans. Deep-Sea Res. 56, 554–577. https://doi.org/10.1016/j.dsr2.2008.12.009.

Takahashi, T., Sutherland, S.C., Kozyr, A., 2013. Global Ocean surface water partial pressure of CO2 database: measurements performed during 1957–2012 (version 2012). In: ORNL/CDIAC-160, NDP-088(V2012). Carbon Dioxide Information Analysis Center, Oak Ridge National Laboratory, U.S. Department of Energy, Oak ridge, Tennessee. https://doi.org/10.3334/CDIAC/OTG.NDP088(V2012).

Takahashi, T., Sutherland, S.C., Chipman, D.W., Goddard, J.G., Newberger, T., Sweeney, C., 2014. Climatological distributions of pH, pCO_2, Total CO_2, alkalinity, and $CaCO_3$ saturation in the global Surface Ocean. In: ORNL/CDIAC-160, NDP-094. Carbon Dioxide Information Analysis Center, oak Ridge National Laboratory, U.S. Department of Energy, Oak Ridge, Tennessee. https://doi.org/10.3334/CDIAC/OTG.NDP094.

Takahashi, T., Sutherland, S.C., Kozyr, A., 2017. Global Ocean surface water partial pressure of CO_2 database. In: Measurements Performed during 1957–2018 (LDEO Database Version 2018) (NCEI Accession 0160492). Version 3.3. NOAA National Centers for Environmental Information. Dataset.

Thomas, W.H., 1966. On denitrification in the northeastern tropical Pacific Ocean. Deep-Sea Res. Ocean. Abs. 13, 1109–1114. https://doi.org/10.1016/0011-7471(66)90702-9.

Trucco-Pignata, P.N., Hernández-Ayón, J.M., Santamarina-del Ángel, E., Bier, E., Sánchez-Velasco, L., Godínez, V., Norzagaray, O., 2019. Ventilation of the upper oxygen minimum zone in the coastal region off Mexico: implications of El Niño 2015–2016. Front. Mar. Sci. 6, 459. https://doi.org/10.3389/fmars.2019.00459.

Valsala, V., Maksyutov, S., 2010. Simulations and assimilation of global pCO_2 and air-sea CO_2 fluxes using ship observations of surface ocean pCO_2 in a simplified biogeochemical offline model. Tellus 62B, 821–840.

Walker Brown, C., Boutin, J., Mervilat, L., 2015. New insights into FCO_2 variability in the tropical eastern Pacific Ocean using SMOS SSS. Biogeosciences 12, 7315–7329. https://doi.org/10.5194/bg-12-7315-2015.

Wanninkhof, R., 1992. Relationship between wind speed and gas exchange over the ocean. J. Geophys. Res. 5, 7373–7382. https://doi.org/10.1029/92JC00188.

Wanninkhof, R., 2014. Relationship between wind speed and gas exchange over the ocean revisited. Limnol. Oceanogr. 12, 351–362. https://doi.org/10.4319/lom.2014.12.351.

Yasunaka, S., Nojiri, Y., Nakaoka, S., Ono, T., Mukai, H., Usui, N., 2014. North Pacific dissolved inorganic carbon variations related to the Pacific decadal oscillation. Geophys. Res. Lett. 41, 1005–1011.

Weiss, R.F., 1974. Carbon dioxide in water and seawater: the solubility of a non-ideal gas. Marine Chem 2 (3), 203–215.

Yasunaka, S., Kouketsu, S., Strutton, P., Murata, A., Nakaoka, S., Nojiri, Y., 2019. Spatio-temporal variability of surface water pCO_2 and nutrients in the tropical Pacific from 1981 to 2015. Deep-Sea Res. Part II, 169–170. https://doi.org/10.1016/j.dsr2.2019.104680.

Zhang, S., Tian, W., 2019. The impacts of modeling global CO_2 concentrations with GEOS-Chem using different ocean carbon fluxes. Atm. Ocean. Sci. Lett. 12, 343–348. https://doi.org/10.1080/16742834.2019.1631690.

Journal Online

Journal of Marine Systems -Scopus 2022

Journal of Marine Systems Scopus details in 2022.

This web page will help you to find Scopus details for the journal **Journal of Marine Systems** and other details.
More specifically, check the current **Scopus indexing status** of the Journal of Marine Systems. Moreover, you can also check the ranking status (if applicable) like SJR, CiteScore, SNIP, and Quartile.

Journal of Marine Systems Metrics: Quartile, CiteScore

The quartile ranking of Journal of Marine Systems is Q1.

CiteScore	4.8
SNIP	1.089
SJR	0.828
Quartile	Q1

CiteScore of an academic journal is a measure reflecting the yearly average number of citations to recent articles published in that journal.

Each subject category of journals is divided into four quartiles: Q1, Q2, Q3 & Q4. Q1 means ranking among the top 25% of journals in the same field.

Important details of Journal of Marine Systems

Journal Title	Journal of Marine Systems
Publisher	Elsevier BV
P-ISSN	9247963
Current Scopus Status	Active
Coverage	1990-ongoing
Article	ENG
Source Type	Journal

Journal of Marine Systems Scopus indexing 2022

Journal Online

Is Journal of Marine Systems Scopus indexed in 2022?

Yes, the **Journal of Marine Systems** is Scopus indexed. The Scopus coverage period of Journal of Marine Systems is 1990-ongoing.

Journal of Marine Systems publication fee

Please visit official website of Journal of Marine Systems to know the publication fee of the journal.

An article processing charge (APC), also known as a publication fee, is a fee which is sometimes charged to authors. Most commonly, it is involved in making a work available as open access (OA), in either a full OA journal or in a hybrid journal.

About Scopus

Scopus is Elsevier abstract and citation database launched in 2004. Scopus covers nearly 36,377 titles (22,794 active titles and 13,583 inactive titles).

All journals covered in the Scopus database are reviewed for sufficiently high quality each year according to four types of numerical quality measure for each title; those are h-Index, CiteScore, SJR (SCImago Journal Rank) and SNIP (Source Normalized Impact per Paper).

How to publish in Scopus journals?

1. Identify a Scopus indexed Journal.
2. Compose Your Research Paper As Per The Guidelines Of The Journal.
3. Visit the journal's website to submit your research paper.
4. Notification Of Acceptance From The Publisher.
5. Confirmation Of Your Paper Being Published

How do I check/ find my Scopus indexed journals?

Visit to the Homepage, and enter the journal title to check the current Scopus indexing status for the journal.

Similarily, the Journal Online's homepage will help you in finding suitable Scopus, SCI journals.

Journal Online

Journals

- [Agricultural Sciences]
- [Arts & Humanities]
- [Business, Management & Accounting]
- [Chemistry]
- [Computer Science]
- [Dentistry]
- [Economics & Finance]
- [Engineering]
- [Health]
- [Mathematics]
- [Medicine]

Journal Online

- Physics & Astronomy
- Social Sciences